

T.C.
TURKISH-GERMAN UNIVERSITY
INSTITUTE OF THE GRADUATE STUDIES
IN SCIENCE AND ENGINEERING

ADDITIVE MANUFACTURING AND MECHANICAL PROPERTIES OF OPEN-PORE
RESIN FOAM STRUCTURES DEVELOPED BY IMAGE PROCESSING ON THE
COMPUTED TOMOGRAPHY DATA

Master's Thesis

Nouh RASTANAWI

ISTANBUL 2023

T.C.
TURKISH-GERMAN UNIVERSITY
INSTITUTE OF THE GRADUATE STUDIES
IN SCIENCE AND ENGINEERING

ADDITIVE MANUFACTURING AND MECHANICAL PROPERTIES OF OPEN-PORE
RESIN FOAM STRUCTURES DEVELOPED BY IMAGE PROCESSING ON THE
COMPUTED TOMOGRAPHY DATA

Master's Thesis

Nouh RASTANAWI

M.Sc., Program Name Turkish-German University, 2023

Advisor
Asst. Prof. Ali Can KAYA

Submitted to the Institute of the Graduate Studies in
Science and Engineering in partial fulfillment of the requirements for the
Master's degree

ISTANBUL 2023

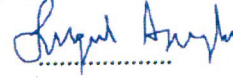
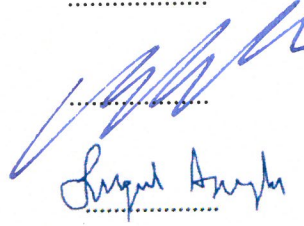
ADDITIVE MANUFACTURING AND MECHANICAL PROPERTIES OF OPEN-PORE
RESIN FOAM STRUCTURES DEVELOPED BY IMAGE PROCESSING ON THE
COMPUTED TOMOGRAPHY DATA

APPROVED BY:

Asst. Prof. Ali Can KAYA
(Thesis Advisor)

Prof. Dr. Yunus Ziya ARSLAN
Türk-Alman Üniversitesi

Asst. Prof. Birgül Aşçıoğlu Temiztaş
Yıldız Teknik Üniversitesi



DATE OF APPROVAL: 22 June 2023

ACKNOWLEDGMENTS

I would also like to thank the committee members Asst. Prof. Ali Can KAYA, Prof. Dr. Yunus Ziya ARSLAN and Asst. Prof. Birgöl Aşçiođlu Temiztaş for their time and attention.

I would like to express my appreciation to my advisor, Asst. Prof. Ali Can KAYA, for their exceptional guidance throughout this thesis. And Lecturer Ali KORUCU as well. Thanks to Asst. Prof. Ali CAN KAYA an article version of the thesis has been published on ScienceDirect.

DECLARATION OF AUTHENTICITY

I declare that I completed the master thesis independently and used only the materials that are listed. All materials used, from published as well as unpublished sources, whether directly quoted or paraphrased, are duly reported. Furthermore, I declare that the master's thesis, or any abridgment of it, was not used for any other degree-seeking purpose and give the publication rights of the thesis to the Institute of the Graduate Studies in Science and Engineering, Turkish-German University.

A handwritten signature in black ink, appearing to read 'Nauh', enclosed within a large, thick, hand-drawn oval.

Nauh RASTANAWI

22.06.2023

ABSTRACT

ADDITIVE MANUFACTURING AND MECHANICAL PROPERTIES OF OPEN-PORE RESIN FOAM STRUCTURES DEVELOPED BY IMAGE PROCESSING ON THE COMPUTED TOMOGRAPHY DATA

Data conversion from computed tomography (CT) data of materials has been widely used for modeling. However, the physical production of open-cell foams through CT data has rarely been conducted for foams. Here we aim to create novel foam structures using image processing on the CT data commercially available foam to enhance energy absorption properties by modifying the deformation mechanisms. In this study, with the use of additive manufacturing techniques such as Masked Stereolithography Apparatus (MSLA), a set of foams were created from computed tomography data of the commercially available steel foams. The sets are 10ppi (pores per inch), 3ppi, merged (10ppi combined with 3ppi) and 10ppi eroded. Testing using quasi-static compression has been used to characterize the mechanical performance and properties of the foams. Grading density decreases the densification strain and increases the plateau regime's slope. The best energy absorption capacity, specific strength, and densification strain were demonstrated by combined foams at high relative densities. 3ppi, 10ppi and 10ppi density-graded foams deform by bending of struts. The bending-dominated structure transformed into a stretch-dominated structure in the case of merged foams. Furthermore, because structures may be remanufactured with the same cell/strut dimensions and imperfections, additively generated resin foams have less mechanical property scattering than conventionally manufactured metal foams.

Keywords: *resin foams; computed tomography; 3D printing; reverse engineering; compression; open cell foams; MSLA.*

ÖZET

BILGISAYARLI TOMOGRAFI VERİLERİ ÜZERİNDE GÖRÜNTÜ İŞLEME YOLUYLA GELİŞTİRİLMİŞ AÇIK GÖZENEKLI REÇİNE KÖPÜKLERİNİN EKLEMELI İMALATI VE MEKANİK ÖZELLİKLERİ

Malzemelerin bilgisayarlı tomografi (BT) verilerinden veri dönüştürme, modelleme için yaygın olarak kullanılmaktadır. Bununla birlikte, BT verileri aracılığıyla açık hücreli köpüklerin fiziksel üretimi köpükler için nadiren gerçekleştirilmiştir. Burada, deformasyon mekanizmalarını değiştirerek enerji soğurma özelliklerini geliştirmek için ticari olarak mevcut köpük BT verileri üzerinde görüntü işleme kullanarak yeni köpük yapıları oluşturmayı amaçlıyoruz. Bu çalışmada, Maskeli Stereolitografi Aparatı (MSLA) gibi eklemeli üretim teknikleri kullanılarak, piyasada bulunan çelik köpüklerin bilgisayarlı tomografi verilerinden bir dizi köpük oluşturulmuştur. Bu setler 10ppi (inç başına gözenek), 3ppi, birleştirilmiş (10ppi ile 3ppi birleştirilmiş) ve 10ppi aşındırılmıştır. Yarı statik sıkıştırma kullanılarak yapılan testler, köpüklerin mekanik performansını ve özelliklerini karakterize etmek için kullanılmıştır. Yoğunluğun derecelendirilmesi, yoğunlaşma gerinimini azaltır ve plato rejiminin eğimini artırır. En iyi enerji emme kapasitesi, özgül mukavemet ve yoğunlaşma gerilmesi, yüksek bağıl yoğunluklarda birleştirilmiş köpükler tarafından gösterilmiştir. 3ppi, 10ppi ve 10ppi yoğunluk dereceli köpükler, dikmelerin bükülmesiyle deforme olur. Eğilme baskın yapı, birleştirilmiş köpükler durumunda gerilme baskın bir yapıya dönüşmüştür. Ayrıca, yapılar aynı hücre/dikme boyutları ve kusurlarla yeniden üretilebildiğinden, katkılı olarak üretilen reçine köpükler, geleneksel olarak üretilen metal köpüklere göre daha az mekanik özellik dağılımına sahiptir.

Anahtar Sözcükler: *reçine köpükler; bilgisayarlı tomografi; 3D baskı; tersine mühendislik; açık hücreli köpükler; MSL*

TABLE OF CONTENTS

ACKNOWLEDGMENTS	IV
DECLARATION OF AUTHENTICITY	V
ABSTRACT.....	VI
ÖZET	VII
LIST OF FIGURES	II
LIST OF TABLES	IV
LIST OF ABBREVIATIONS.....	V
1. INTRODUCTION	1
2. STATE OF THE ART	3
2.1 Additive manufacturing	3
2.2 Reverse engineering	4
2.3 Manufacturing methods	5
2.4 Resin	6
2.5 Relationship between density and strength of foams.....	8
3. METHOD	9
3.1 Reconstruction the 3D models from CT data	10
3.2 Resin 3D printing	20
3.3 Material testing	27
3.4 Compression testing.....	31
3.5 Tensile testing	34
3.6 Data Visualizing & interpretation.....	37
4. FRACTURE OBSERVATIONS	40
5. RESULTS	42
6. DISCUSSION.....	46
7. CONCLUSION	52
8. REFERENCES	54

LIST OF FIGURES

Figure 1	Main steps of this study's method
Figure 2	some of the 30ppi images (raw)
Figure 3	importing the 30ppi CT dataset to Fiji
Figure 4	making a subset of the 30ppi data in Fiji
Figure 5	a) using transform to rotate In Fiji b) an image after rotation
Figure 6	cropping the entire 30ppi dataset
Figure 7	final results of 30ppi
Figure 8	final result of 45ppi
Figure 9	Fiji image calculator
Figure 10	a) 3ppi slice add to b) 10ppi slice to form c) merged sliced
Figure 11	Slicing the merged sample in Chitubox
Figure 12	printing settings used in the study
Figure 13	Archimedes' method to determine density
Figure 14	The used Phrozen Sonic 4K in this study
Figure 15	printed 10ppi sample
Figure 16	Curing a 3ppi sample
Figure 17	10ppi sample
Figure 18	3ppi sample
Figure 19	10ppi eroded sample
Figure 20	two merged (10ppi+3ppi) samples
Figure 21	Shimadzu AGX TM -V2
Figure 22	10ppi sample compression test
Figure 23	eroded sample compression progress
Figure 24	3ppi sample compression progress
Figure 25	10ppi sample compression progress
Figure 26	merged sample compression progress
Figure 27	Printed ASTM 638 tensile specimen
Figure 28	Washed and cured tensile specimen

Figure 29 ASTM 638 resin specimen tensile testing

Figure 30 Specific stress, strain graph for 3ppi

Figure 31 Specific stress, strain graph for 10ppi

Figure 32 Specific stress, strain graph for eroded

Figure 33 Specific stress, strain graph for merged-1

Figure 34 a) Mean stress-strain and b) specific stress-strain curves
of printed 3, 10ppi, density graded, and merged resin foams.

Figure 35 SEM micrograph of damaged strut

Figure 35 SEM micrograph of damaged strut

Figure 36 samples ductility ratio

Figure 36 samples ductility ratio

Figure 37 samples normalized peak stress

Figure 37 samples normalized peak stress

Figure 38 foam cells of a) 3ppi b) 10ppi and c) merged

Figure 38 foam cells of a) 3ppi b) 10ppi and c) merged

Figure 39 a) curve fitting of merging foams' experimental results b)
Comparison of the Gibson-Ahby rule (eq.1) for all tested foams and the
derived equation (eq.3) for merged foams

Figure 39 a) curve fitting of merging foams' experimental results b)
Comparison of the Gibson-Ahby rule (eq.1) for all tested foams and the
derived equation (eq.3) for merged foams

Figure 40 Layers printing direction

Figure 40 Layers printing direction

Figure 41 layer positioning in relation to a strut node's strut section
in an open cell foam

Figure 41 layer positioning in relation to a strut node's strut section
in an open cell foam

LIST OF TABLES

Table 1	10ppi samples data
Table 2	3ppi samples data
Table 3	merged samples data
Table 4	10ppi eroded samples data
Table 5	10ppi samples density values
Table 6	3ppi samples density values
Table 7	merged samples density values
Table 8	10ppi eroded samples density values
Table 9	Mechanical properties of the polymeric resin foams

LIST OF ABBREVIATIONS

CT	Computed Tomography
PPI	Pores Per Inch
MSLA	Masked Stereolithography Apparatus
SLA	Stereolithography
FDM	Fused Deposition Modeling
SLS	Selective Laser Sintering
SLM	Selective Laser Melting
UTS	Ultimate Tensile Strength
CAD	Computer-aided Design

1. INTRODUCTION

The rapid advancement of materials science and engineering has revolutionized various industries, ranging from aerospace and automotive to construction and electronics. Among the multitude of materials developed, resin foams have emerged as versatile and high-performance materials, finding applications in insulation, packaging, and structural components. Traditional methods of resin foam synthesis involve a meticulous process of trial and error, relying on experimental iterations to achieve desired properties. However, recent breakthroughs in reverse engineering techniques have opened up new possibilities for the precise design and synthesis of resin foams with tailored properties. This master thesis aims to explore the realm of reversed engineered resin foams, delving into the principles, methodologies, and applications of this innovative approach. By unraveling the intricacies of reverse engineering resin foams, this research seeks to provide invaluable insights for the development of advanced materials with enhanced performance.

Metal foams are a class of lightweight, porous materials that are composed of metallic alloys. They can be formed using various methods depending on the desired properties and applications of the foam. Common methods include powder metallurgy, where metal powders are mixed with a foaming agent and compressed into a preform; gas injection, where a gas is injected into a molten metal to create bubbles; melt foaming, where a metal is melted and a blowing agent is added to the molten metal; and electrochemical deposition, where metal ions are reduced at the surface of a substrate. These methods each have their own advantages and limitations and can be used to create metal foams with controlled pore sizes, shapes and structure, suitable for a variety of applications. This unique structure provides foams with a range of desirable properties, including high strength-to-weight ratio, excellent energy absorption, and good thermal insulation. Metal foams can be made from a variety of metals and alloys, such as aluminum, magnesium, titanium, and steel, and can be tailored to meet specific performance requirements. And due to their unique properties, metal foams have a wide range of applications across various industries, including aerospace, automotive, biomedical, and energy.

Some of the key applications of metal foams are:

1. **Structural materials:** Metal foams are lightweight and strong, making them ideal for structural applications in aerospace and automotive industries. They can be used to create lightweight and crash-resistant parts such as bumpers, fenders, and body panels in vehicles. Metal foams can also be used in aerospace applications such as structural panels, heat shields, and fuel tank baffles.
2. **Thermal insulation:** Metal foams have excellent thermal insulation properties and can be used as insulation materials in high-temperature applications such as furnaces, kilns, and boilers.
3. **Energy absorption:** Metal foams are excellent energy absorbers and can be used in impact protection applications such as helmets, sports gear, and packaging materials. They can also be used in structural applications such as earthquake-resistant building materials.
4. **Biomedical implants:** Metal foams can be used as implant materials in biomedical applications due to their biocompatibility, lightweight, and mechanical properties. They can be used for bone and tissue regeneration, dental implants, and prosthetic devices.
5. **Sound absorption:** Metal foams can be used as sound-absorbing materials in acoustic insulation applications such as music studios, concert halls, and automotive interiors.

These are just a few examples of the many applications of foams. With their unique properties, metal foams have the potential to revolutionize various industries and contribute to the development of new technologies. [1-7]

In general, SLA-fabricated polymeric resin foams with free ends exhibit typical foam behavior in compression: an elastic initial loading line is followed by a three-long extended plateau regime caused by foam cell collapse and crushing, which is followed by a densification regime where cells compact with nearby cells. Contrarily, Bi et al. also showed that foams with two plates attached on both ends did not exhibit an extended plateau regime and catastrophically ruptured.[8]

The failure behavior of the struts is a topic of discussion in relation to the polymeric resin foams. Celzard et al.'s demonstration that cell collapse was fracture-dominated rather than bending-dominated prompted questions concerning the brittle carbon struts' dominant failure behavior. [25]

Here, we want to improve energy absorption qualities by altering the deformation mechanisms of commercially available foam by creating novel foam structures utilizing image processing on the CT data. In method chapter, more about the method that was used to conduct the experiments is discussed.

2. STATE OF THE ART

In this study, the way is used to create the foams' structure is by using digital design methods. The field of reversed-engineered resin foams has witnessed significant progress, positioning it at the forefront of materials research and development. This master thesis contributes to the state of the art by providing a comprehensive analysis of the latest advancements, methodologies, and insights in the realm of reversed-engineered resin foams.

2.1 Additive manufacturing

Additive manufacturing (AM), also known as 3D printing, is a revolutionary technology that has transformed the manufacturing landscape. It involves the creation of three-dimensional objects by adding material layer by layer, based on a digital design. Unlike traditional manufacturing methods that rely on subtractive processes like cutting or drilling, additive manufacturing builds objects from the ground up, enabling unprecedented design flexibility and complexity. This technology has found applications across various industries, from aerospace and automotive to healthcare and consumer products. It allows for rapid prototyping, cost-effective production of customized products, and the ability to create intricate geometries that were previously unachievable. With its potential to reduce waste, shorten supply chains, and enable decentralized manufacturing, additive manufacturing has opened up new frontiers of innovation and is poised to revolutionize the way we produce and consume goods. [28-29]

With additive manufacturing processes it is possible to create novel complex structure for the foams. Complex and nearly net-shaped cellular materials may now be manufactured thanks to improvements in additive manufacturing techniques, which also expand their design space. For instance, lattice metamaterials and uniform and graded open-cell foams made of photopolymer were fabricated by stereolithography (SLA), fused deposition modeling (FDM), and selective laser sintering (SLS). Laser powder bed fusion or electron beam melting techniques were used to create the metallic equivalent of polymer foams. Due to the layer-by-layer construction of parts using additive manufacturing techniques, samples' microstructures exhibit anisotropic behavior that affects the mechanical characteristics of metals and polymers. Moreover, local melting and cooling cause residual stresses in the materials that control their mechanical properties in additive manufacturing processes. The connection between the process parameters and the mechanical characteristics of additively produced bulk materials is still being studied in great detail. Due to the small size of the struts in foam structures, size and scale effects are present, and the random orientation of the struts with respect to the building direction results in peculiar deformation behavior. [7-15]

2.2 Reverse engineering

Reverse engineering with additive manufacturing combines the power of both technologies to recreate or enhance existing objects or systems. By utilizing 3D scanning technologies, reverse engineering allows for the precise capture of the physical dimensions and geometry of an object. The scanned data can then be imported into computer-aided design (CAD) software, where it can be manipulated, modified, or optimized as needed. With the flexibility and freedom offered by additive manufacturing, the recreated or enhanced object can be produced layer by layer, replicating the original design or incorporating improvements based on the reverse engineering analysis. This approach is particularly beneficial when dealing with complex or intricate parts that may be challenging to reproduce using traditional manufacturing methods. Reverse engineering with additive manufacturing enables industries to extend the lifespan of legacy components, create spare parts, enhance performance, and explore design variations, ultimately opening up a world of possibilities for innovation and optimization.

Today, 3D scanning technologies have become more precise and efficient, allowing for the accurate capture of complex geometries and fine details. High-resolution scanners, such as laser scanners and structured light scanners, provide fast and accurate point cloud data, which can be directly integrated into CAD software for reverse engineering purposes.

Additive manufacturing technologies have also made significant strides, with advancements in materials, printing techniques, and machine capabilities. The availability of a wide range of materials, including metals, polymers, ceramics, and composites, allows for the replication of diverse objects and the creation of functional prototypes or end-use parts. Additive manufacturing processes, such as selective laser sintering (SLS), fused deposition modeling (FDM), and stereolithography (SLA), deliver high precision, intricate details, and improved surface finishes, further enhancing the accuracy and quality of reverse engineered parts.

Overall, the state of the art in reverse engineering with additive manufacturing showcases a synergistic combination of advanced 3D scanning technologies, sophisticated software tools, and enhanced additive manufacturing capabilities. These advancements have significantly improved the efficiency, accuracy, and versatility of reverse engineering, allowing industries to leverage the benefits of additive manufacturing to recreate, enhance, and innovate upon existing objects or systems. [30-31]

2.3 Manufacturing methods

Stereolithography (SLA):

SLA is a 3D printing method that uses a liquid resin that is cured by a light source, typically a UV laser, layer by layer. The resin is contained in a tank, and a platform gradually lifts the object out of the resin as each layer is cured. SLA is known for its high level of detail, smooth surface finishes, and ability to produce intricate geometries. It is suitable for applications like jewelry, dental models, and product prototypes. SLA can achieve high resolution and accuracy, allowing for the creation of precise and visually appealing parts. However, the process requires post-processing steps such as rinsing and UV curing to remove excess resin and ensure the final part's mechanical properties. [32-33]

Fused Deposition Modeling (FDM):

FDM is an additive manufacturing method that works by extruding thermoplastic materials through a heated nozzle. The material, usually in the form of filament, is fed into the printer and melted to a semi-liquid state. It is then deposited layer by layer onto a build platform, where it quickly solidifies. FDM is known for its simplicity and affordability, making it widely used in various industries and for rapid prototyping applications. It offers a range of thermoplastic materials to choose from, including ABS, PLA, PETG, and more. FDM printers are relatively easy to operate, making them popular among hobbyists, educators, and small businesses. [34-35]

Selective Laser Sintering (SLS):

SLS is a powder-based additive manufacturing method where a laser selectively fuses powdered material, typically polymers or metals, layer by layer. The process involves spreading a thin layer of powder onto a build platform and using a laser to selectively heat and fuse the particles, solidifying the desired shape. SLS allows for the production of complex and functional parts with high strength and durability. It does not require support structures since the surrounding powder acts as a self-supporting medium during the printing process. This makes SLS suitable for creating intricate and interlocking designs. The variety of materials available for SLS includes nylon, TPU (thermoplastic polyurethane), and even metal powders, enabling a wide range of applications such as functional prototypes, end-use parts, and customized products. [36-38]

Selective Laser Melting (SLM):

SLM is a metal-based additive manufacturing method that uses a high-powered laser to selectively melt and fuse metal powder particles layer by layer. It is similar to SLS but specifically designed for metal materials. The process creates fully dense and highly accurate metal parts with excellent mechanical properties. SLM is widely used in industries such as aerospace, automotive, and medical where complex metal components with high structural integrity are required. By melting the metal powder at high temperatures, SLM allows for the production of parts with intricate geometries and internal structures that are difficult or impossible to achieve through traditional manufacturing methods. It offers a range of metal materials, including stainless steel, titanium alloys, aluminum alloys, and more, providing versatility for various industrial applications. [37-38]

These additive manufacturing methods offer different capabilities, material compatibilities, and cost considerations, making them suitable for various applications across industries. It's important to choose the appropriate method based on the desired outcome, material requirements, and the specific needs of the project. Additionally, it's worth noting that continuous advancements in additive manufacturing technologies continue to expand the range of materials, processes, and applications available in the field.

2.4 Resin

Resins used for 3D printing, specifically in processes like stereolithography (SLA) and digital light processing (DLP), are photopolymer materials that undergo a photochemical reaction when exposed to specific wavelengths of light. These resins are typically liquid or viscous in form and contain a combination of monomers, oligomers, photoinitiators, and additives.

When a light source, such as a UV laser or projector, emits light onto the resin, the photoinitiators within the resin absorb the light energy and initiate a polymerization process. This process causes the liquid resin to solidify or cure, transforming it from a liquid state to a solid, layer by layer.

Resins for 3D printing come in various types and formulations, each with its own specific properties and characteristics. For example, there are resins tailored for high-resolution applications that offer fine details and smooth surface finishes. Others are designed to be flexible or elastomeric, allowing for the creation of rubber-like or flexible parts. There are also resins available with different colors, transparency levels, and material properties such as hardness or heat resistance.

Here are some common types of SLA resins:

1. **Standard Resins:** These are general-purpose resins suitable for a wide range of applications. They offer good strength, detail resolution, and surface finish. Standard resins are often used for prototypes, functional parts, and visual models.
2. **Engineering Resins:** These resins are formulated with enhanced mechanical properties, such as increased strength, heat resistance, or impact resistance. Engineering resins are commonly used for functional prototypes, jigs, fixtures, and parts that require higher durability or specific mechanical characteristics.
3. **Flexible Resins:** These resins produce parts with rubber-like flexibility and elasticity. They are ideal for creating objects that require bending, compressing, or flexing properties. Flexible resins find applications in areas like robotics, wearable devices, and ergonomic prototypes.
4. **Castable Resins:** These specialized resins are designed for creating models and molds for investment casting processes. They burn out cleanly without leaving residue, making them suitable for jewelry making, dental applications, and other industries that require precise casting.
5. **High-Temperature Resins:** These resins are formulated to withstand elevated temperatures without deformation or degradation. They are commonly used in applications like molds, jigs, and fixtures for high-temperature processes or functional parts exposed to heat.
6. **Dental Resins:** These resins are specifically formulated for dental applications, including dental models, orthodontic devices, and surgical guides. They offer biocompatibility and accuracy required for dental applications.
7. **Transparent Resins:** These resins produce clear or translucent parts with high optical clarity. They are used when transparency or light transmission is desired, such as for prototyping light guides, lenses, or other transparent objects.
8. **Specialty Resins:** There are also specialty resins available with specific characteristics, such as high impact resistance, flame retardancy, or biocompatibility for medical applications. These resins cater to specific industry needs and specialized applications.

9. **Water-Washable Resin:** Water-Washable Resin is exactly what the name says it is. This material stands out for simple and easy post-processing with water instead of using IPA (Isopropyl Alcohol) or anything similar. Apart from its ease of use, this resin boasts a low odor and higher strength than Standard Resin. However, it's quite brittle as well, thanks to the gradual water absorption by the part as you clean and post-process it with water.

It's important to note that different 3D printing technologies may require specific resins compatible with their respective processes. Therefore, it's crucial to select the appropriate resin type and formulation that is compatible with the specific 3D printer and printing method being used. [40]

2.5 Relationship between density and strength of foams

The relationship between density and strength in foams can be complex and is influenced by various factors. Here are some general observations regarding the relationship between density and strength in foams:

1. **Compressive Strength:** In most cases, there is a positive correlation between foam density and compressive strength. Higher-density foams tend to have higher compressive strength. This is because a higher density means a greater number of cells and interconnections, which can distribute and absorb compressive forces more effectively. The increased cell density provides more structural integrity, making the foam less prone to collapsing or deforming under compression.
2. **Tensile Strength:** The relationship between density and tensile strength in foams is not as straightforward as in compressive strength. While increasing density can improve tensile strength to some extent, it is not always a direct correlation. Other factors such as the foam composition, cell wall thickness, and foam structure play significant roles in determining tensile strength.
3. **Shear Strength:** Similar to tensile strength, the relationship between density and shear strength in foams is influenced by various factors. Higher-density foams generally exhibit higher shear strength due to their increased structural integrity. However, other factors such as the foam composition, cell structure, and foam type can also affect shear strength.

It's important to note that the relationship between density and strength in foams can be influenced by several factors beyond just density. The specific foam composition, cell structure (open-cell or closed-cell), cell size and shape, foam processing parameters, and the nature of the foam material itself can all impact the strength characteristics. Additionally, factors like the type and distribution of load, the direction of force application, and the environmental conditions under which the foam operates can also affect its strength properties.

3. METHOD

The process that is used to conduct the study and get the result will be in four main steps, a brief telling of the process should be: starting with having the computed tomography (CT) data of which the foams' structure will be reversed-engineered made and then a rendering and creating of the 3D models out of the CT data. After that they are ready to be printed. Once the cuboid specimens that are produced available comes the quasi-static compression to test the parts mechanically and see how they will perform. Images of the resin struts' fracture surfaces were captured using optical (OM) and secondary electron microscope (SEM) techniques. It was also shown how the topology modifications affected the foams' strength and ductility ratio later on. More detailed is as follows:

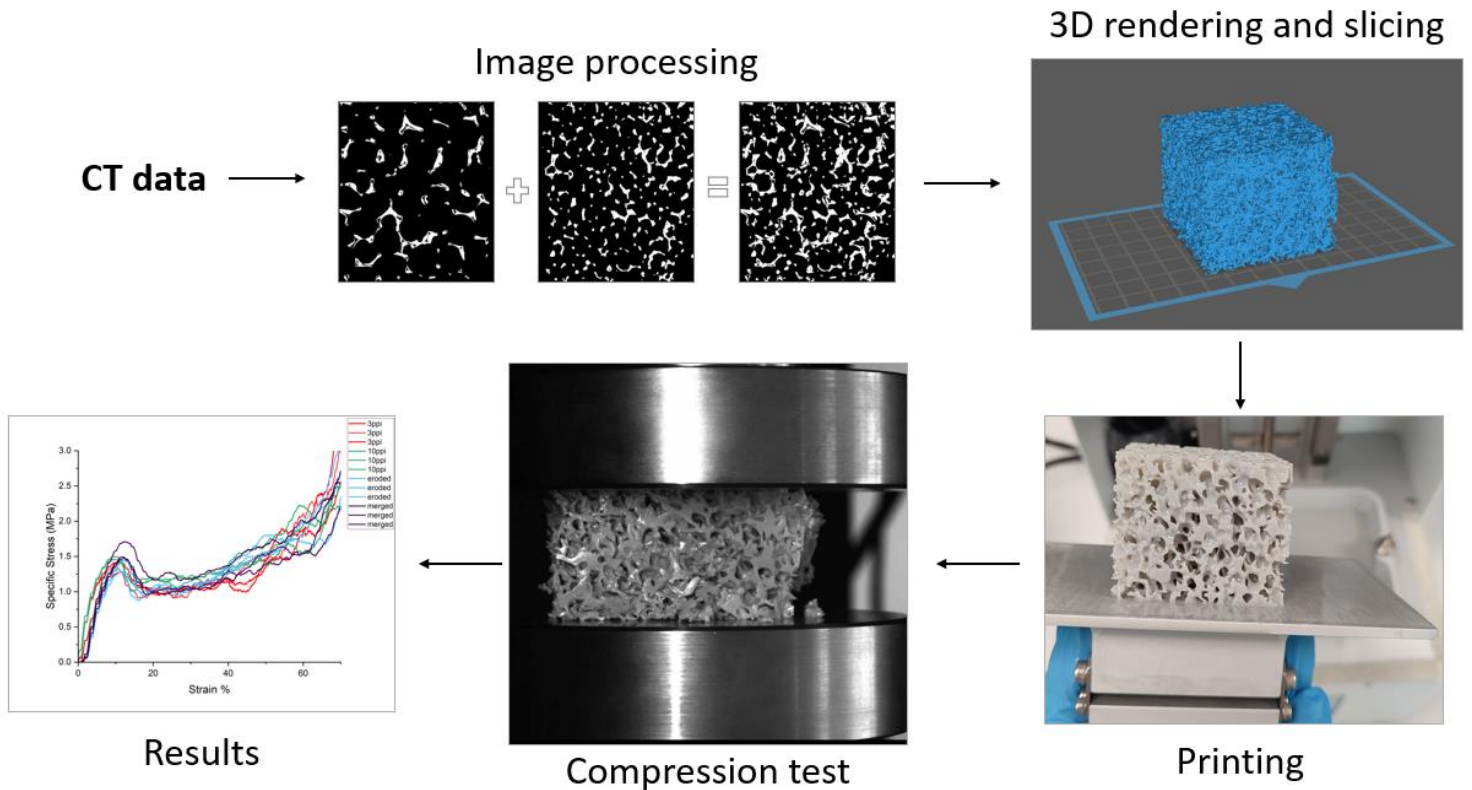


Figure 1 Main steps of this study's method

3.1 Reconstruction the 3D models from CT data

CT imaging can also be utilized to study and analyze materials that incorporate foams, including metallic foams. In this context, CT scanning provides valuable insights into the internal structure, porosity, and distribution of foam within the material. By subjecting a foam-containing sample to a CT scan, X-ray beams pass through the material and interact differently with the foam and surrounding components. The X-rays are attenuated differently by the foam due to its lower density, resulting in variations in the detected X-ray intensity. These intensity variations are then processed by the computer to generate a 3D representation of the foam structure within the material. CT imaging of foams in materials offers numerous advantages. It allows for the non-destructive examination of foam distribution, connectivity, and defects. The visualization of the internal foam structure aids in assessing the quality and integrity of foam-based materials, enabling researchers and engineers to optimize their design and manufacturing processes. Furthermore, CT scans can provide valuable data for characterizing the mechanical properties of metallic foams. By correlating the foam structure revealed by CT imaging with mechanical testing, researchers can analyze the foam's deformation behavior, determine its load-bearing capacity, and assess its performance in various applications. In summary, CT imaging plays a crucial role in analyzing and understanding metallic foams embedded within materials. It enables researchers to visualize the internal structure, evaluate the foam's distribution and quality, and gain insights into its mechanical behavior. These capabilities contribute to the advancement of foam-based materials in a wide range of industries, including aerospace, automotive, and biomedical applications. [16][17]

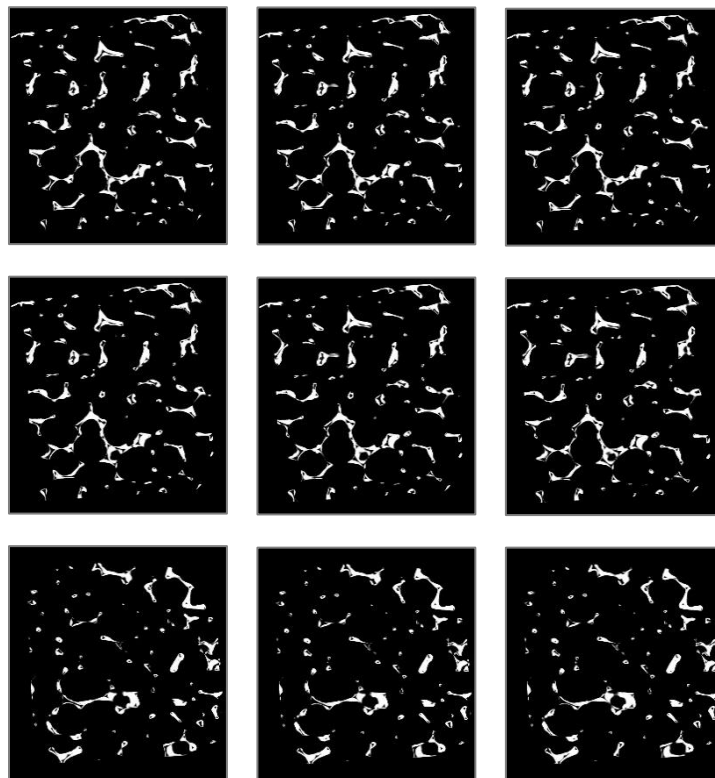


Figure 2 some of the 30ppi images (raw)

The CT data that are worked with in this study to generate the resin foam structure are two datasets of 30ppi and 45ppi images, which are originally reverse-engineered of metal foams, namely, 30 and 45ppi 316L stainless steel foams that were purchased from Hollomet and later on cut into a cuboid size $20 \times 20 \times 20 \text{ mm}^3$. PPI typically refers to the measurement used to determine the density of pores in a material or object. It is commonly used in the context of materials such as foams, filters, or porous membranes. The 30ppi has about 1400 images, while the 45ppi has about 900 images. Since the number of images (slices) of them is different (unequal), a need to make them have the same number of slices is raised. So, the 30ppi and 45ppi's images have to be reduced. To achieve that Fiji was used, which is also known as ImageJ, is a popular open-source image processing package widely used in the scientific and research community. Fiji is designed to handle a wide range of image data, including 2D, 3D, and time-lapse images. It offers a user-friendly interface and supports various file formats commonly used in microscopy and scientific imaging. It is widely utilized in various fields such as biology, bioinformatics, materials science, and medical research for image analysis and quantitative measurements. After opening the program and then import the CT data.

Figure 03 shows us some of the metadata of the set such as dimensions (1341x1419), the stacks number and their size (2.5GB).

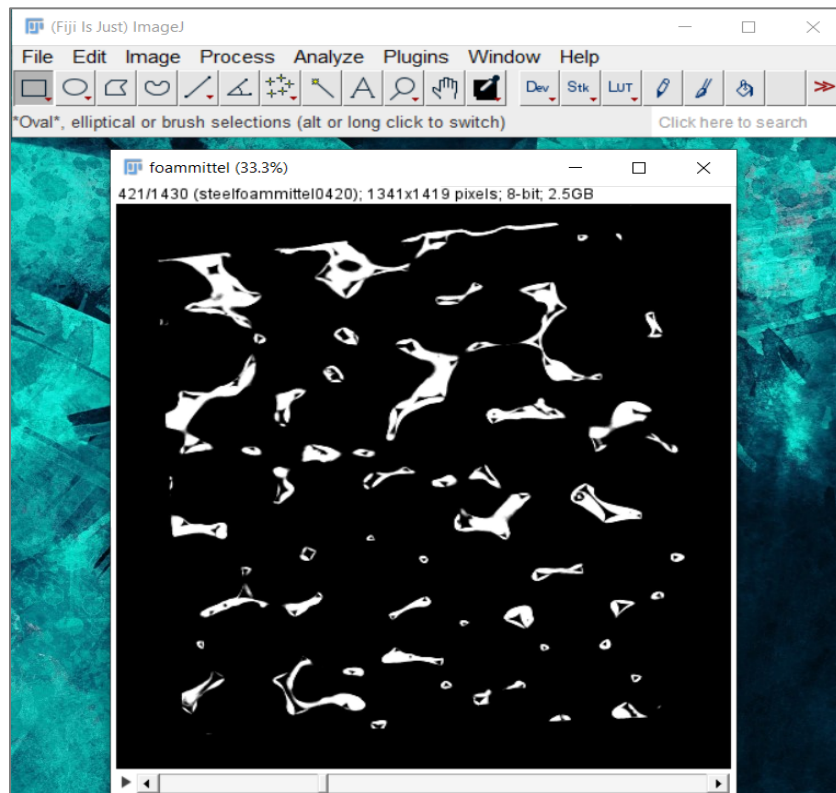


Figure 3 importing the 30ppi CT dataset to Fiji

First, extracting a subset out the foam CT dataset 45ppi and 30ppi is required. The number of images per dataset is now 491 images.

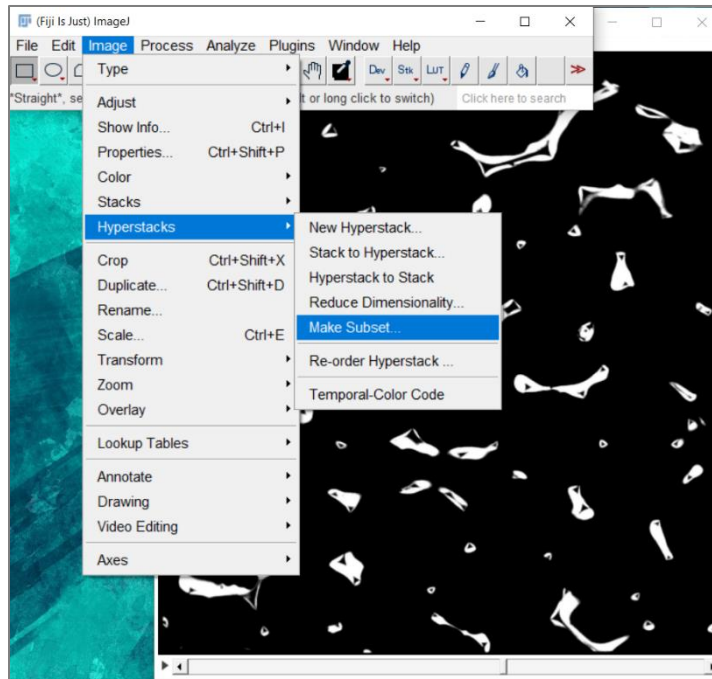


Figure 4 making a subset of the 30ppi data in Fiji

Not finished yet. Some image processing modifications working is still needed. Because the two datasets have different dimensions and 30ppi images have an empty area in the borders and they don't have a straight angle as it visible in figure 02, it is better to perform some cropping and rotation on the images' sequences in this situation.

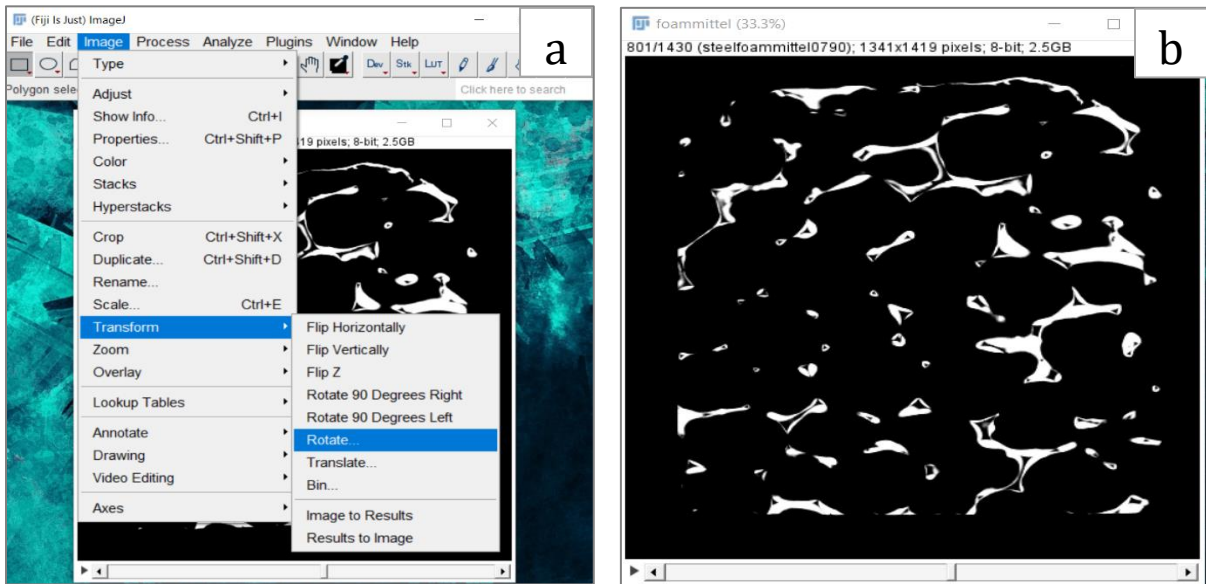


Figure 5 a) using transform to rotate In Fiji b) an image after rotation

Last thing to do now is cropping. The selection should be while keeping as much as possible of the data (the white) and remove the empty areas (the black) considering the same for all the images.

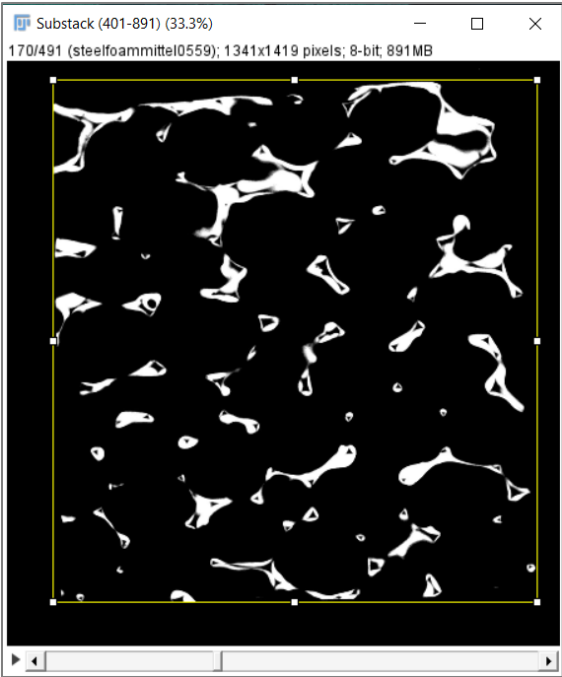


Figure 6 cropping the entire 30ppi dataset

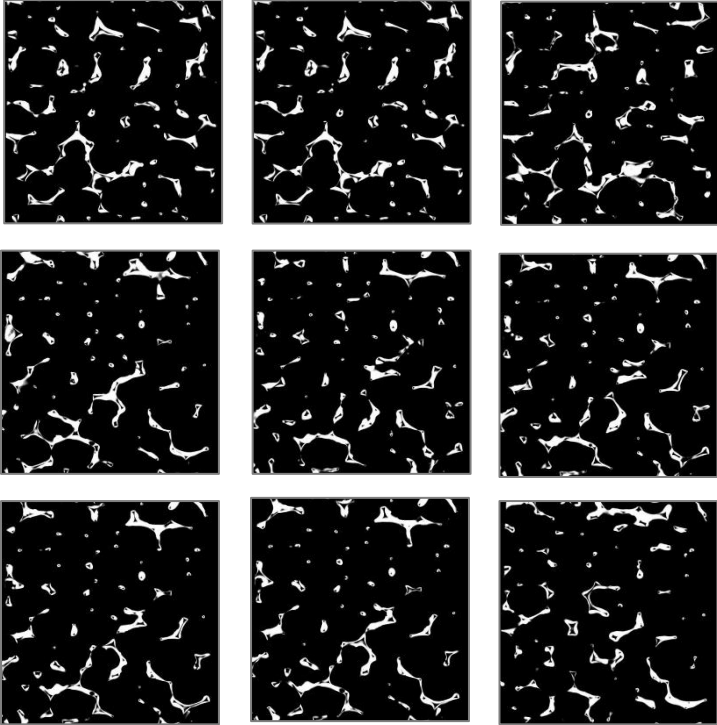


Figure 7 final results of 30ppi

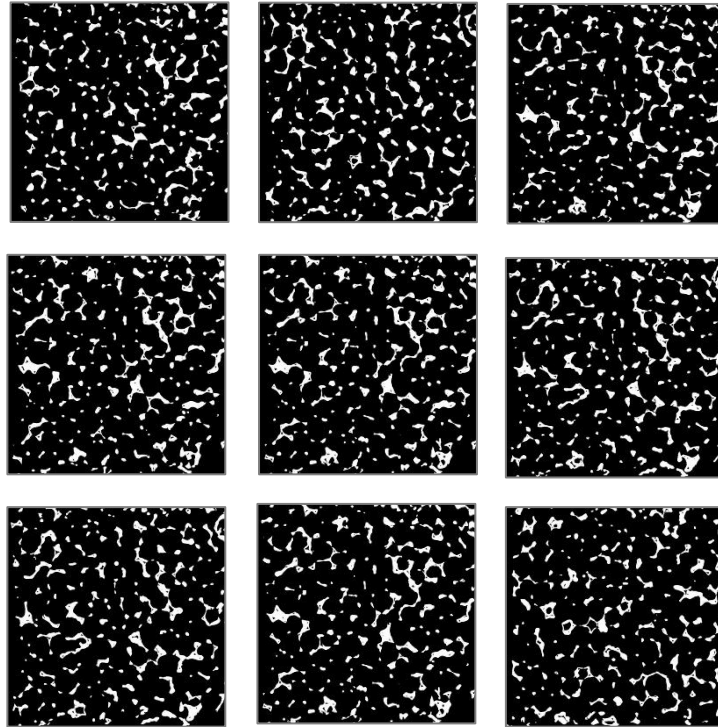


Figure 8 final result of 45ppi

As a consequence of changing the images size from (1341x1419) to (586x586) after cropping them, a redetermination of their new PPI is required. To determine the new PPI of a material, the following steps are for that:

1. Obtain a sample of the material whose pore density you want to measure.
2. Ensure the sample is representative of the material's overall structure and has a sufficient size for accurate measurement.
3. Prepare the sample by cleaning and ensuring it is free from any debris or foreign particles that could interfere with the pore measurement.
4. Use a microscope or a magnification device capable of capturing clear and detailed images of the material's surface.
5. Capture an image of a representative area of the material, ensuring that it includes a sufficient number of pores for accurate measurement.
6. Transfer the captured image to a computer or image analysis software that allows for precise measurement and analysis of the image.

7. Using the image analysis software, select a specific region of interest (ROI) within the captured image that contains a significant number of pores.
8. Count the number of pores within the selected ROI. This can be done manually by visually identifying and counting each pore, or by using automated image analysis algorithms available in the software.
9. Measure the physical length or width of the ROI in inches.
10. Calculate the PPI by dividing the number of pores counted by the length or width of the ROI in inches.

After calculating the new values after printing the samples. The new PPI values are as follows:

45ppi → 10ppi
30ppi → 3ppi

Now the 3D models are ready to be produced out of the two CT datasets. Two 3D test samples can be generated now and to have more different samples that are distinct from the first two, Fiji's image calculator will be used to create more variants as test samples. There are no specific criteria for the other variants, which means that there are so many options for us to choose from. A new dataset can be generated by eroding/dilating the 10ppi's or the 30ppi's or whole new thing by merging the datasets together by using Fiji's image Calculator. Regardless of the choice, the important thing here to observe how it will perform during the compressions test later on. In this study the printed samples will be made out of: 10ppi, 3ppi, 10ppi eroded (Fiji's erode tool is implemented to increase the thickness of the struts by five times along the foam height) and 10ppi added to 3ppi (merged).

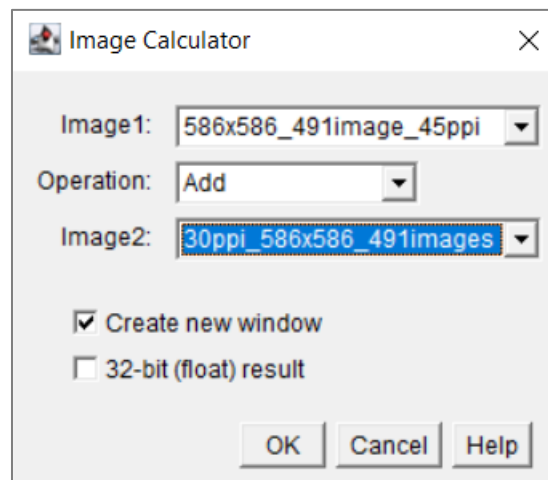


Figure 9 Fiji image calculator

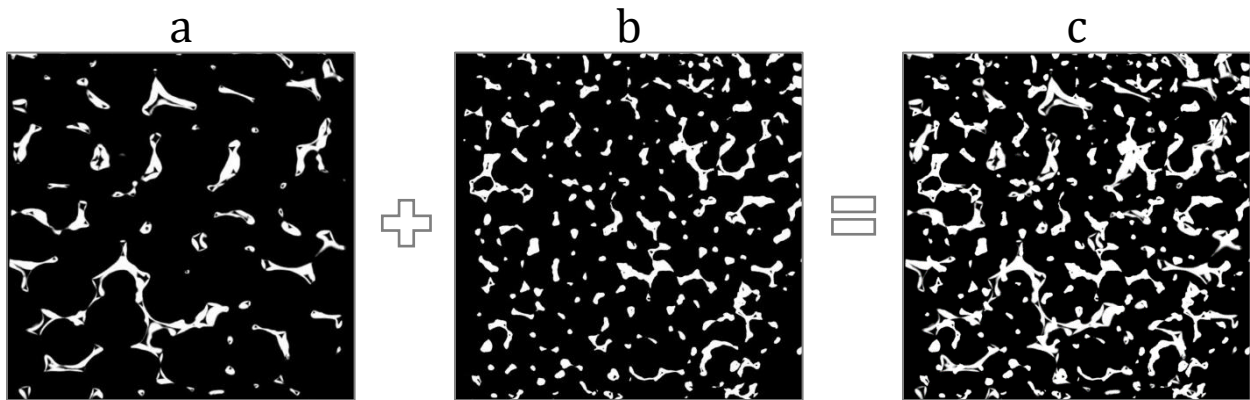


Figure 10 a) 3ppi slice add to b) 10ppi slice to form c) merged sliced

The last step in this section is to turn the produced CT datasets to 3D models and prepare them to be printed, and for that InVesalius is being used. InVesalius is a software application used for medical imaging visualization and processing. It is primarily focused on the field of medical imaging and provides tools for the reconstruction, segmentation, and visualization of medical data. It is well-suited for working with CT (computed tomography) data. In fact, one of the primary applications of InVesalius is to import CT scans and utilize its tools for visualization and analysis of the imaging data.

With InVesalius, you can import CT image data and perform various tasks, such as:

1. **Image Visualization:** InVesalius allows you to view CT scans in different orientations (axial, sagittal, coronal) and manipulate the images to gain a better understanding of the anatomy.
2. **Image Segmentation:** InVesalius provides tools for image segmentation, allowing you to isolate specific anatomical structures or regions of interest from the CT data. This segmentation process can help in generating accurate 3D models of the desired structures.
3. **3D Reconstruction:** InVesalius enables the reconstruction of 3D models from the CT data. By segmenting and manipulating the CT scans, you can create detailed 3D models of anatomical structures or specific regions of interest.

It is of note to mention that InVesalius is a demanding program to use when trying to render the 3D model that are made of a big dataset. Once InVesalius is finished with building the model, it can be exported as an STL file, and then opened in a slicing software.

Chitubox is one of the available recommended choices. Chitubox is a widely used slicing software for resin-based 3D printing. It offers a user-friendly interface and a range of features to prepare 3D models for printing on resin printers. With Chitubox, we can import models in various formats, slice them into layers, and customize support structures to optimize print quality. The software allows for precise orientation of models, and provides tools for editing individual layers and making local adjustments. Chitubox also offers options for hollowing out models and adding drain holes, reducing material usage and facilitating resin removal. It supports anti-aliasing settings for smoother prints and provides control over exposure settings. Compatibility with a wide range of resin printers and the ability to export sliced files make Chitubox a versatile and popular choice for resin-based 3D printing.

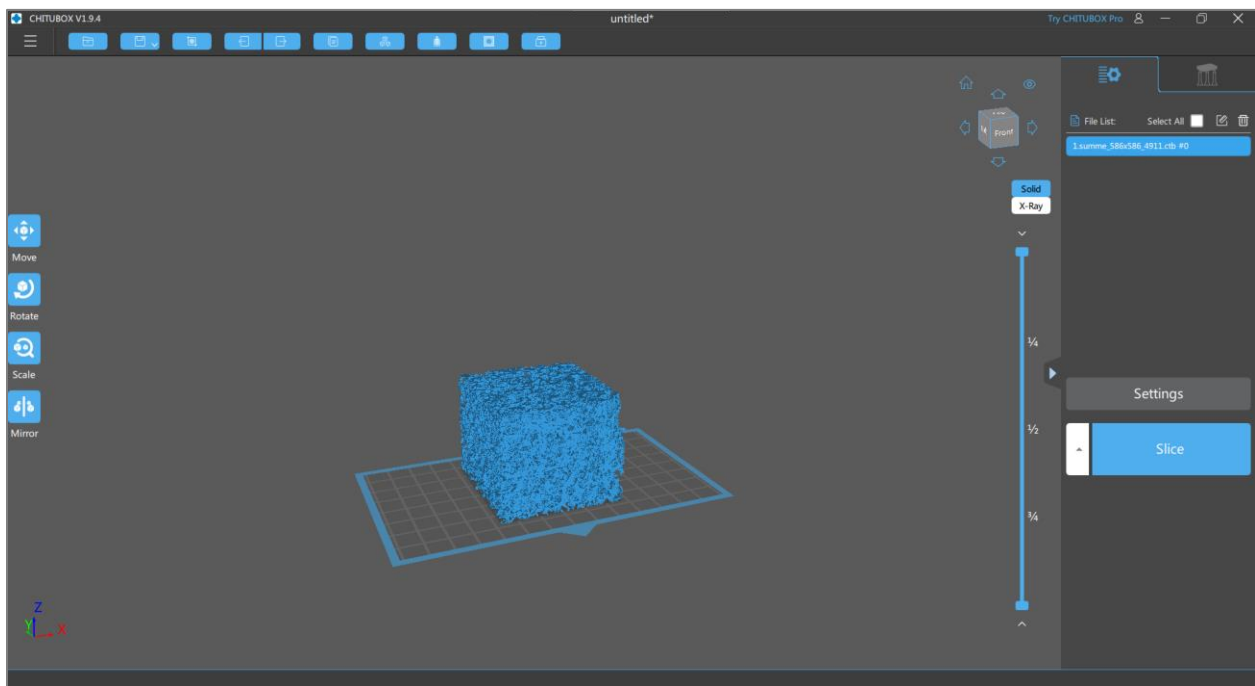


Figure 11 Slicing the merged sample in Chitubox

All of the samples should be followed by the same steps and be sliced with the same settings. Printing settings for resin-based 3D printing can vary depending on factors such as the specific printer model, resin type, desired print quality, and the characteristics of the object being printed.

However, here are some general printing settings that are commonly adjusted:

1. **Layer Height:** This refers to the thickness of each layer that the printer will print. Smaller layer heights generally result in finer details but can increase print time.
2. **Exposure Time:** The exposure time determines how long each layer is exposed to the UV light during the curing process.
3. **Bottom Layer Exposure Time:** The bottom layers of a print often require a longer exposure time to ensure proper adhesion to the build platform. This setting is separate from the regular exposure time.
4. **Lift Height and Speed:** These settings determine how far and how quickly the build plate rises after each layer is cured. They can affect the print quality, especially when dealing with delicate or intricate models.
5. **Print Speed:** The speed at which the printer moves during the printing process. Higher speeds can reduce print time but may sacrifice some print quality.

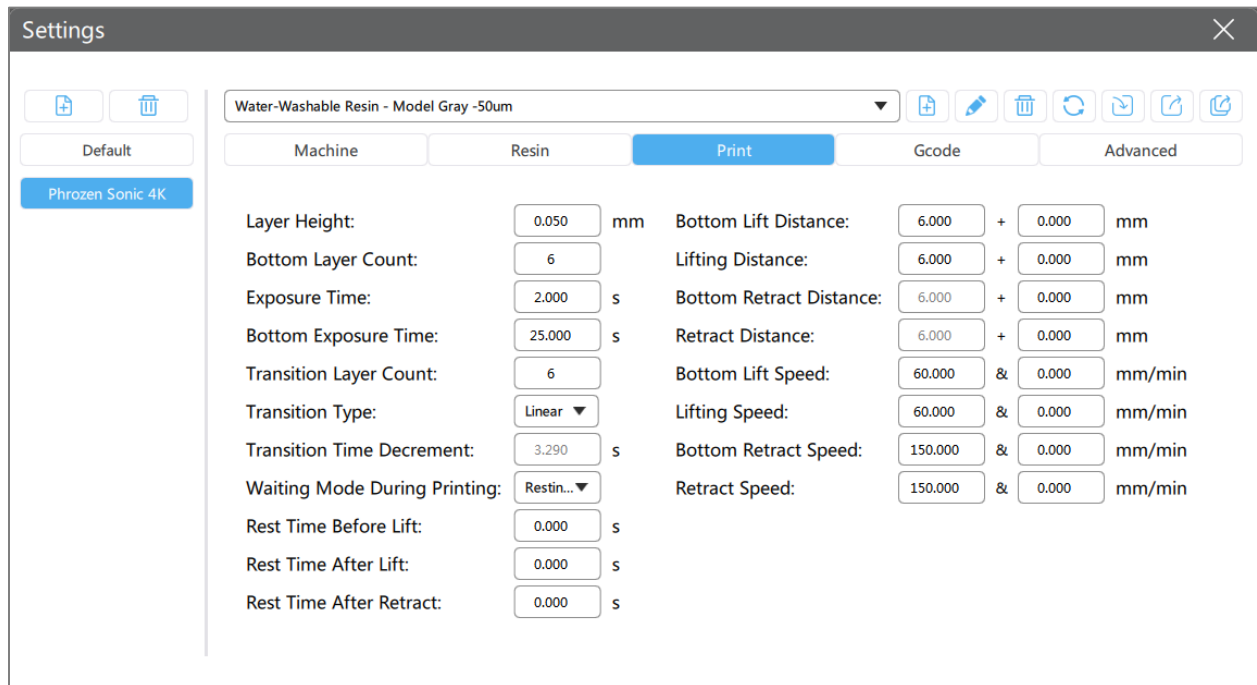


Figure 12 printing settings used in the study

The printed dimension of the resin foams was measured to be $50 \times 50 \times 41 \text{ mm}^3$. Using Archimedes' method, the density of the printed standard tensile resin specimen was determined to be 1.21 g/cm^3 . Archimedes' method to determine density is known as the Archimedes' principle or the method of buoyancy. According to this principle, when an object is submerged in a fluid, it experiences an upward buoyant force equal to the weight of the fluid it displaces. To use this method, first measure the mass of the object using a scale or balance. Then, fill a container with a known volume of fluid, typically water, and measure the volume accurately. Place the container on a scale and record its weight. Next, carefully lower the object into the fluid until it is completely submerged, ensuring there are no air bubbles attached to it. Measure the combined weight of the container, fluid, and the submerged object. Calculate the weight difference between the container with the fluid and the container with the fluid and submerged object. This weight difference represents the buoyant force experienced by the object. Using the buoyant force, determine the weight of the fluid displaced by the object, as the buoyant force is equal to the weight of the displaced fluid. Finally, divide the mass of the object by the volume of the fluid displaced to find the density using the formula $\text{density} = \text{mass} / \text{volume}$. It is important to note that this method assumes full submersion of the object and no chemical reactions between the object and the fluid.

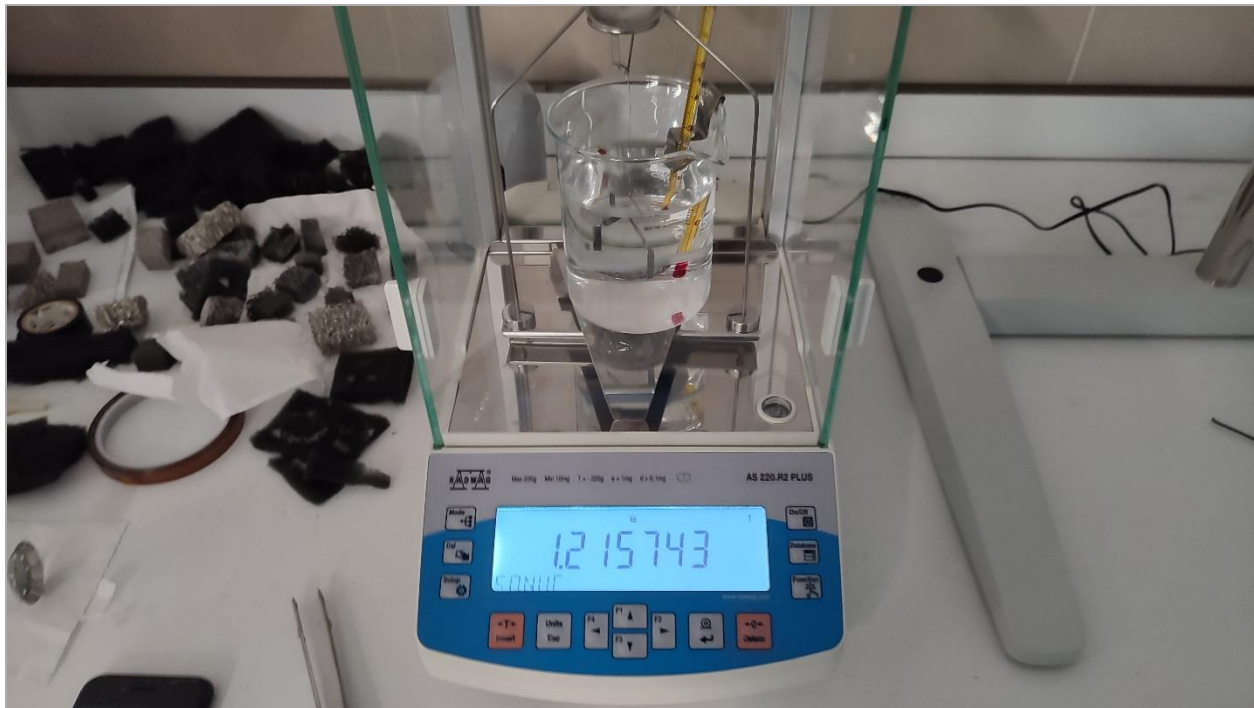


Figure 13 Archimedes' method to determine density

Now, the next step is all set up to be started, which is printing them. The next section will be focused on the printing process.

3.2 Resin 3D printing

The printer that is used to produce the samples is "Phrozen Sonic 4K". It is a high-resolution 3D printer manufactured by Phrozen, a company specializing in resin-based 3D printing technology. Phrozen 3D printers are known for their accuracy and precision in creating detailed resin-based prints. They typically utilize LCD (Liquid Crystal Display) or DLP (Digital Light Processing) technology to cure the resin layer by layer, resulting in high-quality 3D prints.

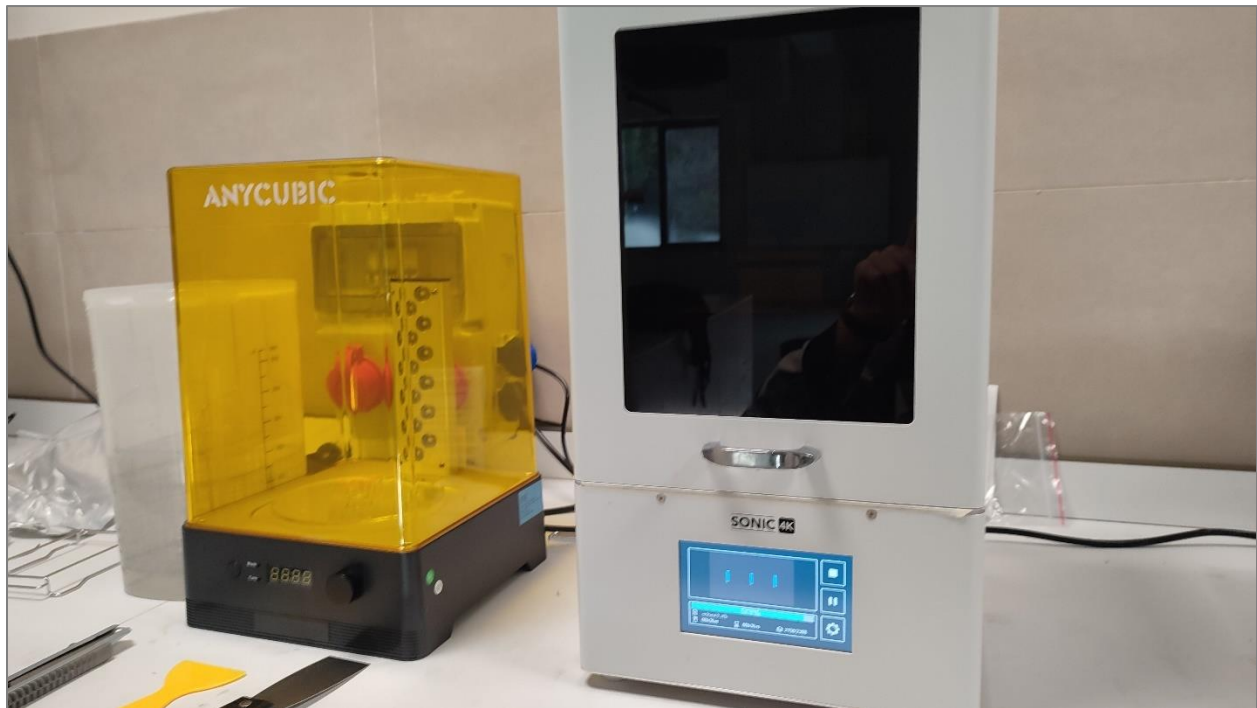


Figure 14 The used Phrozen Sonic 4K in this study

Resin printers, such as SLA (Stereolithography) and DLP (Digital Light Processing) printers, use liquid photopolymer resins as the material for 3D printing. These resins are specially formulated to solidify or cure when exposed to specific wavelengths of light, typically in the ultraviolet (UV) spectrum. Photopolymer resins come in various formulations and properties, allowing for different applications and end results. Some common types of resin materials used in resin printers include:

1. **Standard Resins:** These resins are general-purpose materials suitable for a wide range of applications. They offer good detail resolution and surface finish.
2. **Engineering Resins:** These resins are designed to have specific mechanical properties, such as high strength, toughness, or flexibility. They are often used for functional prototypes or end-use parts that require more robust characteristics.

3. **Dental and Medical Resins:** Resins formulated for dental and medical applications must meet stringent requirements for biocompatibility and accuracy. They are used for creating dental models, surgical guides, orthodontic appliances, and other medical devices
4. **Castable Resins:** These resins are specifically formulated for investment casting applications. They can be burned out cleanly without leaving residue, making them suitable for creating molds for metal casting.
5. **Specialty Resins:** There are also specialty resins available for specific purposes, such as high-temperature resistance, high transparency, or rubber-like flexibility.

It's important to note that different resin printers have specific requirements regarding the type of resin they can use. It's recommended to check the manufacturer's guidelines and recommendations to ensure compatibility between the printer and the resin material you intend to use.

Material:

The material which is used to print all of the polymeric resin foams samples is Water-washable grey resin (Phrozen Tech Co., Hsinchu City, TAIWAN). It is a specific type of resin used in resin-based 3D printers. It is formulated to be easily cleanable with water, eliminating the need for harsh chemicals or solvents for post-processing. The water-washable property of this resin allows users to remove excess uncured resin from printed objects by rinsing them in water. This feature simplifies the cleaning process and reduces the handling of potentially toxic chemicals, making it a more user-friendly option. This polymeric resin is a photocurable resin made up of photoinitiators, diluents, monomers, or oligomers. Liquid polymeric resin has a viscosity of 125 *cP* and a density of 1.1 *g/cm³*, respectively. Grey resin is a common color choice for 3D printing as it provides a neutral base that is suitable for various applications, including prototypes, miniatures, and functional parts. The grey color is also beneficial for highlighting details and surface finishes. It's worth noting that different manufacturers may offer their own water-washable grey resin formulations, so it's advisable to refer to the specific instructions and guidelines provided by the resin manufacturer for optimal printing and post-processing procedures.

Out of each model three samples were produced which will results in 12 samples with four types. Conducting the compression with only one sample is not sufficient. This way will end up with more consistence results. The first model to be printed was the 10ppi model.

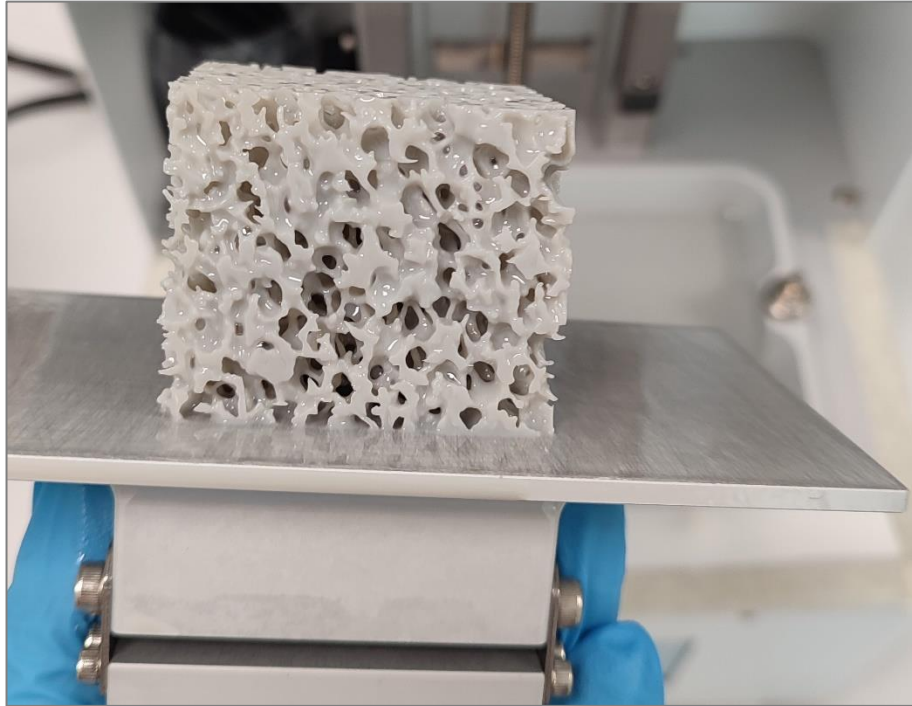


Figure 15 printed 10ppi sample

Washing the printed part after resin-based 3D printing is an important step in the post-processing workflow. It helps to remove excess uncured resin and ensures that the final printed object is clean and ready for further handling or additional post-processing steps.

Here are some reasons why washing the printed part is important:

1. **Removal of uncured resin:** After the 3D printing process, the printed part may still have uncured resin residues on its surface. Washing the part helps to remove these residues, reducing the presence of potentially hazardous or irritating materials.
2. **Enhanced safety:** Resin-based 3D printing involves the use of photopolymer resins that can be sensitive to ultraviolet (UV) light. Washing the part removes any uncured resin that could potentially cause skin irritation or other adverse reactions if left on the printed object.
3. **Improved surface finish:** Washing the part can improve the surface quality of the printed object. It helps to remove any excess resin that may have pooled or accumulated during the printing process, resulting in a smoother surface finish.

4. Better accuracy and dimensional stability: Removing excess resin through washing can also contribute to the dimensional accuracy and stability of the printed part. Excess resin left on the object can affect its dimensions and may lead to warping or distortion if not properly removed.
5. Facilitates further post-processing: Once the part is washed and dried, it is ready for additional post-processing steps such as curing, sanding, painting, or surface finishing. Having a clean and resin-free part ensures that subsequent steps can be performed effectively and produce the desired results.

Following the washing comes the curing. Curing is an essential step in the post-processing of resin-based 3D prints. It involves using a light source, typically UV light, to expose the printed object and initiate the chemical reaction that hardens the resin. Curing ensures that the printed part reaches its final solid state and improves its mechanical properties. Here are some key points about the curing process:

1. Curing Methods: There are different methods for curing resin-based 3D prints. The most common approach is using UV light sources, such as UV LED lamps or UV curing chambers. These emit a specific wavelength of UV light that activates the photoinitiators in the resin and causes it to solidify. Some resins require specific curing conditions, such as exposure to specific wavelengths or intensities of light, so it's important to follow the manufacturer's instructions.
2. Curing Methods: There are different methods for curing resin-based 3D prints. The most common approach is using UV light sources, such as UV LED lamps or UV curing chambers. These emit a specific wavelength of UV light that activates the photoinitiators in the resin and causes it to solidify. Some resins require specific curing conditions, such as exposure to specific wavelengths or intensities of light, so it's important to follow the manufacturer's instructions.
3. Curing Time: The duration of the curing process varies depending on the resin type, the thickness of the printed object, and the chosen curing method. The manufacturer's guidelines typically provide recommendations for the optimal curing time. It's important to ensure that the object receives sufficient exposure to the curing light to ensure complete polymerization.

4. Curing Chamber: For consistent and controlled curing, some 3D printing enthusiasts and professionals use dedicated curing chambers. These chambers provide a controlled environment with evenly distributed UV light to ensure uniform curing of the printed object. Curing chambers are especially useful when printing larger or more complex objects.
5. Post-Curing: Once the initial curing process is complete, it is often recommended to perform post-curing. Post-curing involves subjecting the printed object to additional UV light exposure to further enhance its mechanical properties and ensure complete polymerization. Post-curing can help improve the strength, durability, and stability of the printed part.
6. Safety Precautions: When working with UV light sources for curing, it is important to take safety precautions. UV light can be harmful to the eyes and skin, so it is advisable to wear appropriate protective eyewear and avoid direct exposure to the light during the curing process.

By properly curing resin-based 3D prints, the desired mechanical properties can be achieved and the final solid state of the printed object can be ensured. All of the samples got cured for 10min.

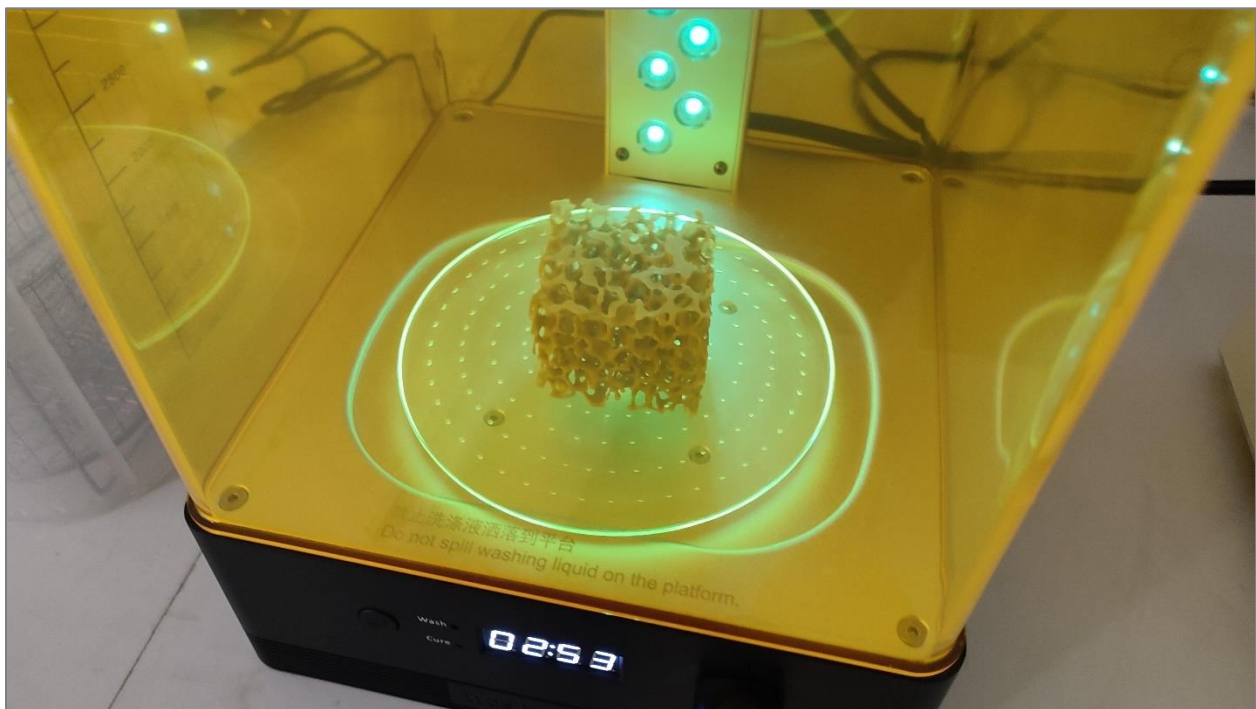


Figure 16 Curing a 3ppi sample

Now, the samples are ready to be tested. Here some pictures of the produced samples in their final shape, washed and cured:

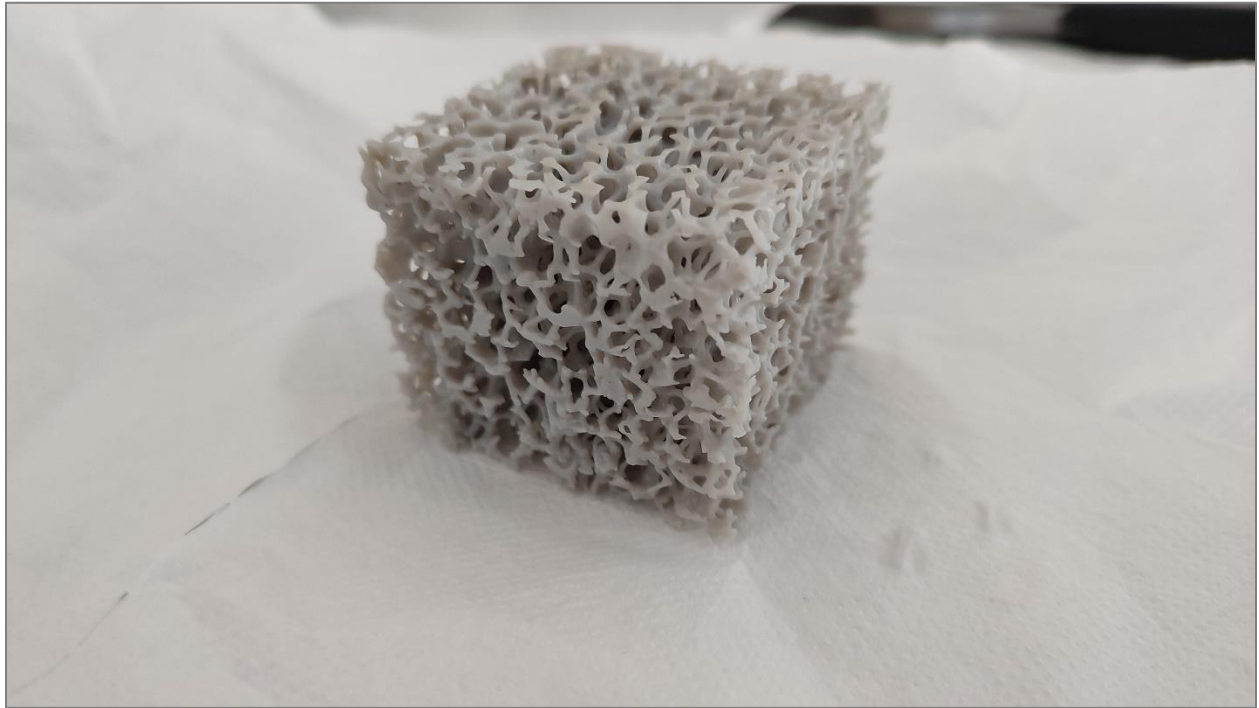


Figure 17 10ppi sample



Figure 18 3ppi sample

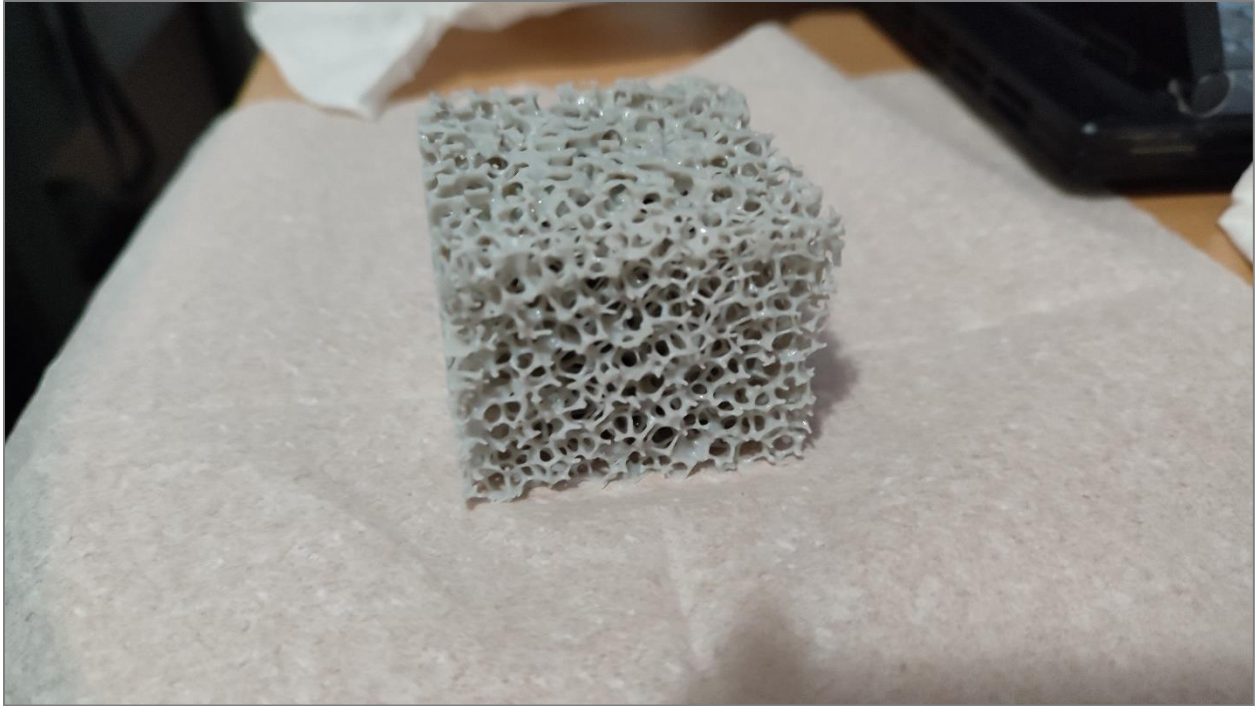


Figure 19 10ppi eroded sample



Figure 20 two merged (10ppi+3ppi) samples

3.3 Material testing

Material testing is a process used to assess and evaluate the properties, performance, and behavior of various materials under different conditions. It involves subjecting the material to controlled tests and experiments to gather data and gain insights into its mechanical, physical, chemical, and thermal properties. Here are some key aspects of material testing:

1. **Test Types:** Material testing encompasses a wide range of tests, each designed to examine specific properties of the material. Common tests include tensile testing, compression testing, flexural testing, hardness testing, impact testing, fatigue testing, creep testing, and thermal analysis.
2. **Mechanical Properties:** Material testing helps determine mechanical properties such as tensile strength, yield strength, modulus of elasticity, toughness, ductility, hardness, and impact resistance. These properties are crucial in understanding how materials respond to external forces or loads.
3. **Physical Properties:** Material testing also investigates physical properties like density, melting point, thermal conductivity, electrical conductivity, coefficient of thermal expansion, and specific heat capacity. These properties provide insights into a material's physical behavior and how it interacts with its surroundings.
4. **Material Characterization:** Through material testing, materials can be characterized to classify them based on their properties. This enables engineers and scientists to select appropriate materials for specific applications and ensure they meet desired specifications.
5. **Quality Control and Assurance:** Material testing is vital in quality control and assurance processes. By conducting regular tests on materials used in manufacturing or construction, companies can ensure that the materials meet required standards and specifications, preventing failures, accidents, or subpar performance.
6. **Research and Development:** Material testing plays a crucial role in research and development efforts. By testing new materials or evaluating existing ones, researchers can understand their capabilities, identify areas for improvement, and optimize materials for specific applications.

Material testing is essential in various fields, including engineering, manufacturing, construction, aerospace, automotive, electronics, and healthcare. It helps in the selection, design, and performance assessment of materials, contributing to the development of safer, more efficient, and higher-quality products and structures.

To evaluate the behavior of materials under compressive loads, compression testing is a common method used for that. It involves subjecting a sample of the material to a compressive force and measuring its response to determine various mechanical properties.

Its primary objective is to evaluate a material's strength, stiffness, and ability to withstand compressive loads without deformation or failure. The test setup involves placing a sample between two compression plates within a testing machine, which gradually applies a controlled axial load to the sample. Throughout the test, the applied force and resulting deformation are measured to construct a stress-strain or load-deformation curve, enabling an understanding of the material's behavior under compressive loading. Important parameters derived from compression testing include compressive strength, which indicates the maximum stress or force the material can withstand before failure, and the elastic modulus, which signifies the material's stiffness within the elastic range. The yield point identifies the stress at which the material undergoes permanent deformation, marking the limit of its elastic behavior. Furthermore, compression testing provides valuable insights into a material's deformation characteristics, such as its ability to recover its original shape after load removal and its tendency to exhibit plastic deformation or failure.



Figure 21 Shimadzu AGX™-V2

Proper sample preparation is essential to ensure accurate and consistent results, including adhering to specific dimensions and surface conditions. That is why all of the test samples have to be measured. Their dimensions as well as their weights. This table below includes all of this data. (Merged set has four samples, because during their compression test one of them had its test stopped in mid of the process and we had to produce another one.)

Table 1 10ppi samples data

10PPI	Mass (g)	X (mm)	Y (mm)	Z (mm)
1 st sample	25.2	50.2	50.3	41.4
2 nd sample	25.1	50.2	50.4	41.4
3 rd sample	25.2	50.2	50.4	41.4

Table 2 3ppi samples data

3PPI	Mass (g)	X (mm)	Y (mm)	Z (mm)
1 st sample	16.7	50.1	49.1	41.3
2 nd sample	17	50.1	49.2	41.4
3 rd sample	17	50.2	49.4	41.2

Table 3 merged samples data

Merged	Mass (g)	X (mm)	Y (mm)	Z (mm)
1 st sample	39.5	50.3	50.3	41.9
2 nd sample	39.1	50.5	50.5	41.9
3 rd sample	39.5	50.6	50.5	41.7
4 th sample	39.5	50.6	50.4	41.9

Table 4 10ppi eroded samples data

10ppi eroded	Mass (g)	X (mm)	Y (mm)	Z (mm)
1 st sample	27	50.5	50.5	41.8
2 nd sample	27.2	50.3	50.5	42
3 rd sample	27.3	50.4	50.2	41.8

After measuring the samples and insert their data, their density was calculated as well. All the required numbers for that are already available. The relative density of the foams (ρ_{rel}) was calculated by dividing the resin density (ρ_f) by the solid density (ρ_s) of the resin. The resin and steel foams' porosity (P) was determined using: $P = 1 - \rho_f/\rho_s$.

Table 5 10ppi samples density values

<i>10ppi</i>	<i>Density</i>	<i>Relative density</i>	<i>Percent</i>	<i>Averaged foam relative density</i>
<i>1st sample</i>	0.240583559	0.198829388	19.8829388	0.198566386
<i>2nd sample</i>	0.239628863	0.198040382	19.80403825	
<i>3rd sample</i>	0.240583559	0.198829388	19.8829388	

Table 6 3ppi samples density values

<i>3ppi</i>	<i>Density</i>	<i>Relative density</i>	<i>Percent</i>	<i>Averaged foam relative density</i>
<i>1st sample</i>	0.159434343	0.13176392	13.17639198	0.133341931
<i>2nd sample</i>	0.162298433	0.134130936	13.41309364	
<i>3rd sample</i>	0.162298433	0.134130936	13.41309364	

Table 7 merged samples density values

<i>Merged</i>	<i>Density</i>	<i>Relative density</i>	<i>Percent</i>	<i>Averaged foam relative density</i>
<i>1st sample</i>	0.377105183	0.311657176	31.16571756	0.31086817
<i>2nd sample</i>	0.373286396	0.308501154	30.85011536	
<i>3rd sample</i>	0.377105183	0.311657176	31.16571756	
<i>4th sample</i>	0.377105183	0.311657176	31.16571756	

Table 8 10ppi eroded samples density values

<i>10ppi eroded</i>	<i>Density</i>	<i>Relative density</i>	<i>Percent</i>	<i>Averaged foam relative density</i>
<i>1st sample</i>	0.257768099	0.213031487	21.30314871	0.214346496
<i>2nd sample</i>	0.259677493	0.214609498	21.46094982	
<i>3rd sample</i>	0.260632189	0.215398504	21.53985037	

Note:

By increasing the thickness of the struts of merged foams, two more foam structures were added to the previous ones to be tested later on. Now there are three types of merged foams: I) Merged-1 (or merged). II) Merged-2. III) Merged-3. The relative density (%) of the new foams was determined to be: 35.0 merged-2 and 42.0 merged-3.

3.4 Compression testing

At this moment, the compression test was commenced. Using a universal testing machine from Shimadzu AGX-V, quasi-static compression testing of foams and tensile testing of standard samples was accomplished (check figure 21). The machine is equipped with a load cell of 100kN and the resolution of 0.5% indicated test force. With a speed accuracy of $\pm 0.1\%$, the crosshead speed was set to 0.08 mm/s. The speed accuracy was calculated from the distance crosshead traveled within a definite time at a constant speed. In order to remove the anisotropic influence of building direction on the mechanical properties, each reverse-engineered resin foam was compressed in the same direction. The compression test results are saved as (csv) file format and they contain the time, force, extension, stress and strain for each test resin sample. A visualization of the data is included in Data collection & Visualizing section so that the results can be readable. [18]

The following photos shows the resin samples as they are compressed in the machine through time from start and how the cells deform.

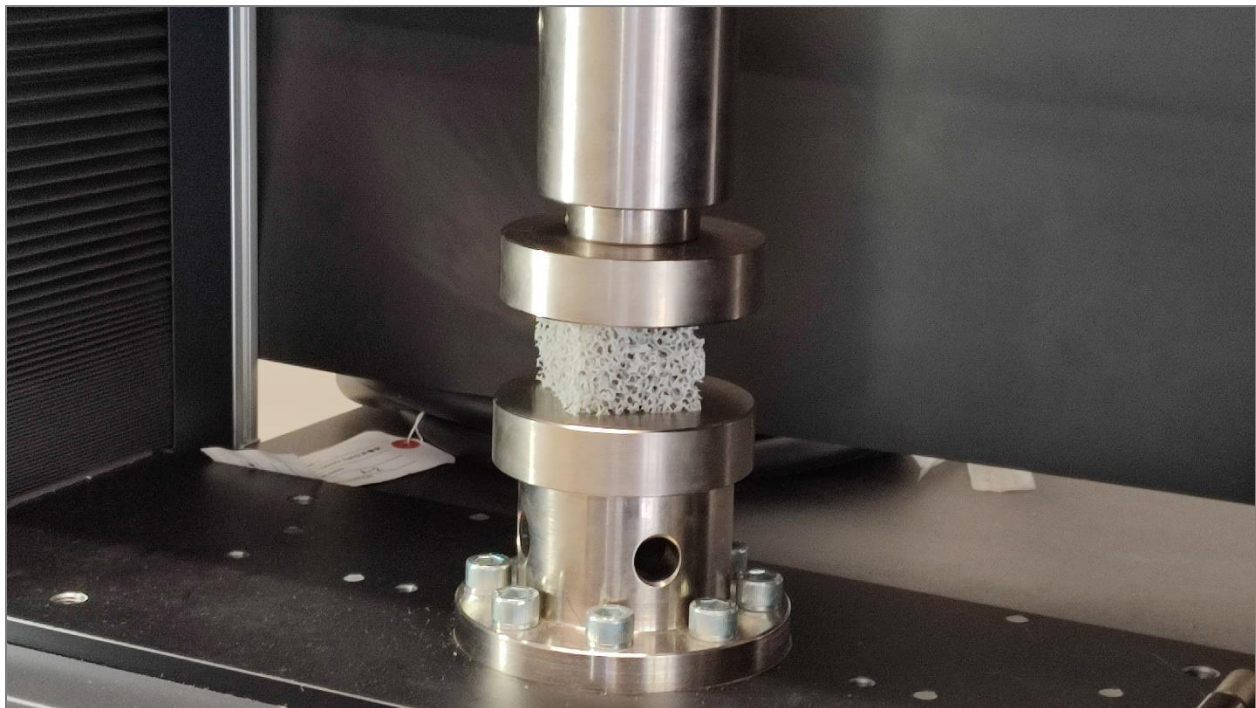


Figure 22 10ppi sample compression test

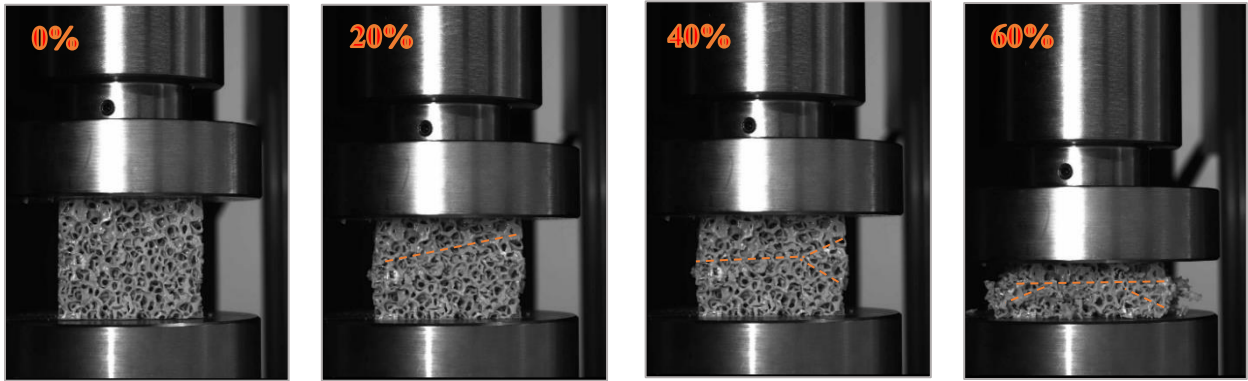


Figure 23 eroded sample compression progress

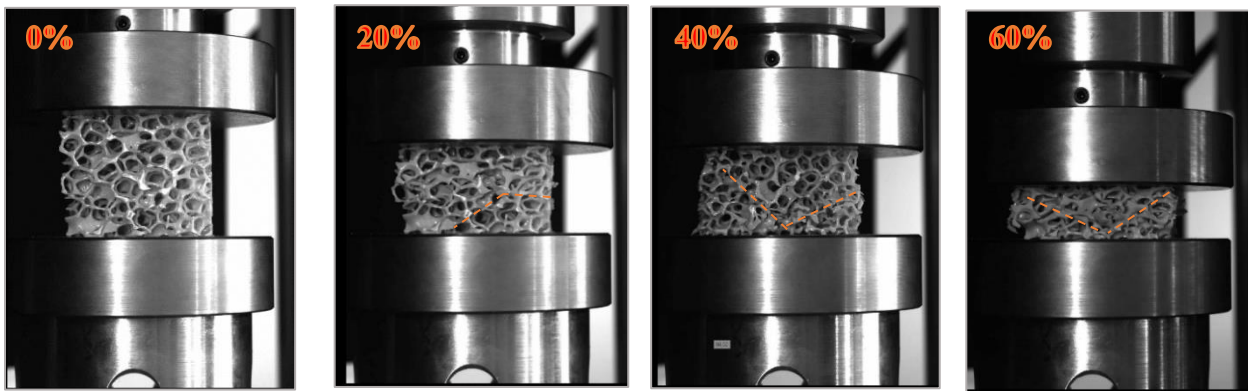


Figure 24 3ppi sample compression progress

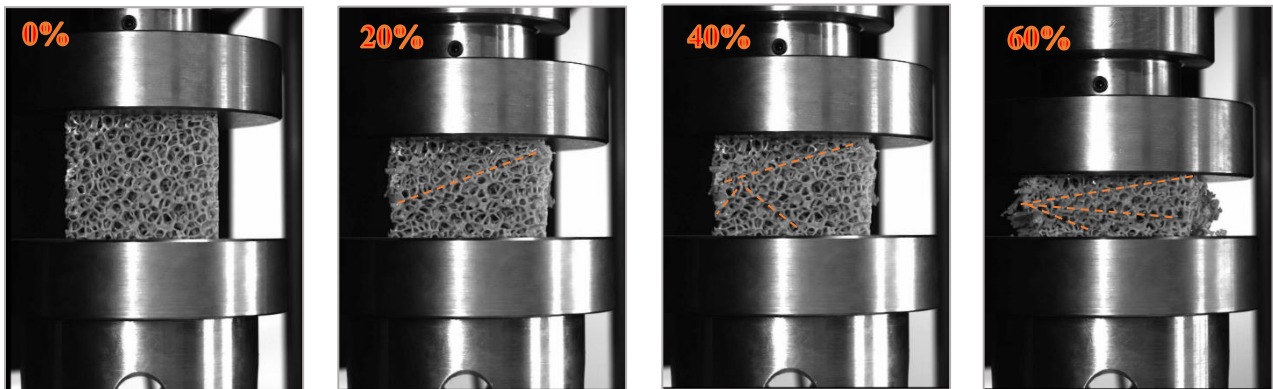


Figure 25 10ppi sample compression progress

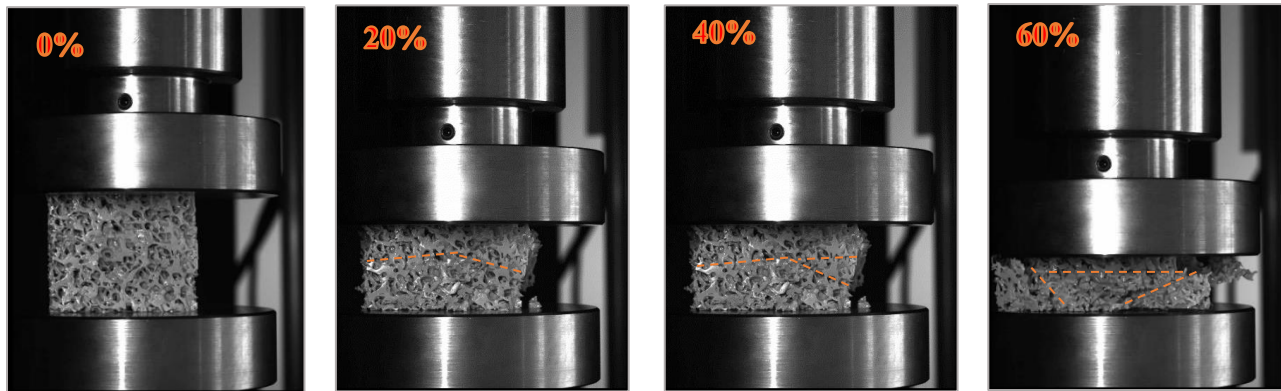


Figure 26 merged sample compression progress

Images taken at 0, 20, 40 and 60% strains show how reverse-engineered resin foams behave when cells collapse under compression. The orange dashed lines indicate deformation bands. The struts' initial bending causes the cells to collapse, and deformation bands. Shear forces cause deformation bands to advance in the case of 3ppi foams. At the beginning strain, bands are created with an acute angle at about 45 degrees and a band parallel to the loading axis. Damage starts out exactly the same for foams with eroded and 10ppi. Deformation bands are created perpendicular to the loading axis tilted at an acute angle in the case of 10ppi and 10ppi eroded (density-graded) foams. The deformation band in the case of merged foams is almost perpendicular to the loading axis. In this instance, a horizontal deformation band in the transverse direction is produced by two adjacent deformation bands that are accompanied by acute angles. The deformation bands get wider as a result of additional cell collapse brought on by damage to the cells in the plateau regime as in to 20% of strain. Other deformation bands with an acute angle of 45 degrees arise in the case of merging foams. The deformation bands multiply when the foam is compressed up to a strain of 40% in the plateau regime. Due to the newly made deformation bands, the stress in the case of 3ppi foams is nearly constant. The cells for merged, graded, and 10ppi foams are compacted, which causes a slight rise in stress. When it comes to graded foams, new deformation bands appear parallel to the bands that have already formed. Shear forces result in merged foams and deformation bands with an acute angle of 45 degrees for 10ppi.

3.5 Tensile testing

Tensile testing, also known as tension testing, is a mechanical testing method used to determine the mechanical properties of a material. It involves subjecting a test specimen to a controlled axial pulling force, or tension, until it fractures or undergoes permanent deformation. The test measures the response of the material to this force, providing valuable information about its strength, ductility, and other mechanical characteristics. Tensile testing is widely used in industries such as manufacturing, construction, automotive, aerospace, and materials research. It helps engineers and researchers understand how materials behave under tension, allowing for material selection, quality control, and design optimization.

Here's an overview of the tensile testing process:

1. **Test Specimen Preparation:** The first step is to prepare the test specimen according to the applicable standards or requirements. The specimen is usually a cylindrical shape with standardized dimensions. It may be machined or obtained from a larger sample, depending on the material and testing standards.
2. **Mounting the Specimen:** The test specimen is securely mounted in the grips of the testing machine. The grips ensure proper alignment and prevent slippage during the test. The machine has two grips, one fixed and one movable, and the specimen is held between them.
3. **Application of Load:** The testing machine applies a tensile load to the specimen in a controlled manner. The load is gradually increased until the specimen fractures or reaches a specified deformation limit. The load is typically applied at a constant rate, known as the strain rate, which is specified in the testing standards.
4. **Measurement of Load and Deformation:** During the test, the testing machine measures both the applied load and the corresponding deformation of the specimen. Load is measured using a load cell, while deformation is measured using an extensometer or other displacement-measuring devices. These measurements help generate a stress-strain curve, which provides insights into the material's behavior.

5. Calculation of Mechanical Properties: From the load and deformation data, various mechanical properties can be calculated. These include:
 - Ultimate Tensile Strength (UTS): The maximum stress the material can withstand before fracturing.
 - Yield Strength: The stress at which the material begins to deform plastically.
 - Elastic Modulus: A measure of the material's stiffness or ability to resist deformation under load.
 - Ductility: The extent to which a material can deform before fracturing, typically measured as elongation or reduction in area.
 - Toughness: The ability of a material to absorb energy before fracture, often represented by the area under the stress-strain curve.

6. Analysis and Interpretation: The test results are analyzed to evaluate the material's performance and compare it with the desired specifications or industry standards.

In the case of tensile testing, CAD software was used to create a 3D CAD model of the ASTM 638 type II tensile specimen. The models in (stl) format were imported into ChituBox and then sliced, and G-Code was generated.



Figure 27 Printed ASTM 638 tensile specimen

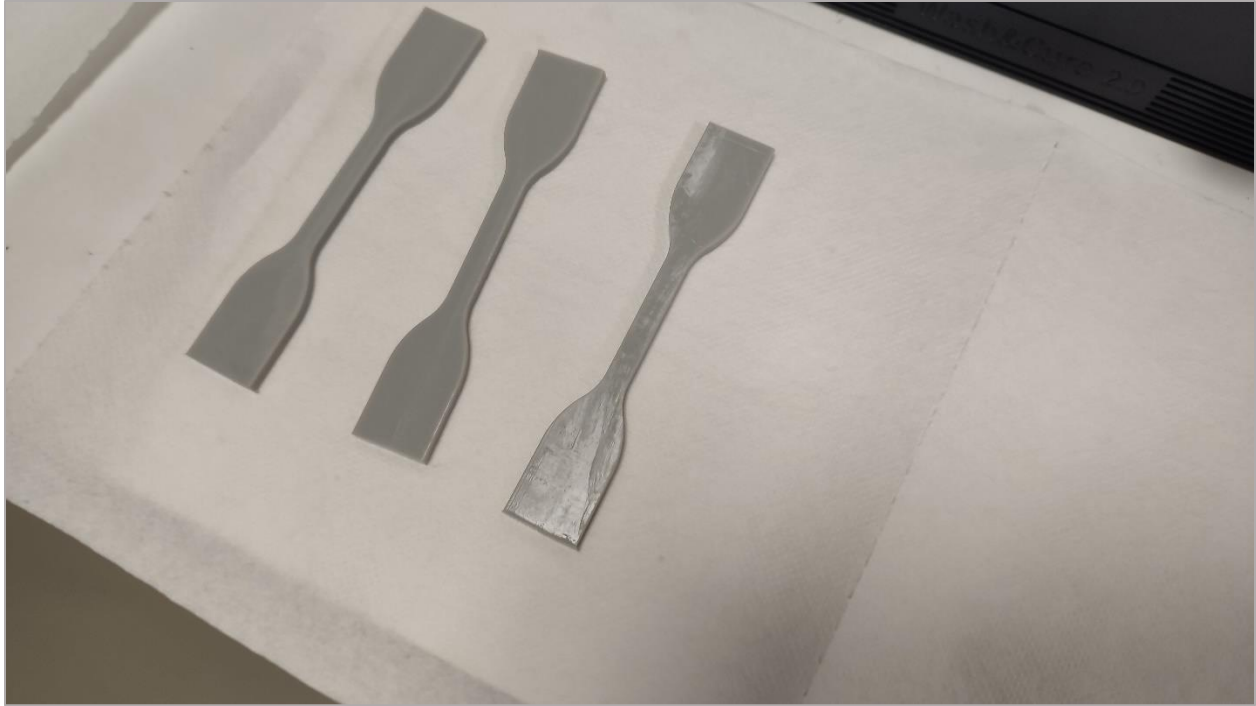


Figure 28 Washed and cured tensile specimen

The specimens were placed upright and built up parallel to the axial direction of the sample. Tensile specimens were pulled with a displacement rate of 5 mm/min. A video extensometer measured the elongation of the samples. The yield strength of the standard bulk resin samples was measured at the fracture point.



Figure 29 ASTM 638 resin specimen tensile testing

3.6 Data Visualizing & interpretation

All of the resin foam stress-strain curves revealed a 10% initial nonlinear elastic regime (fig 30-34). The elastic regime between the 0 and 10 % strain is followed by an extended plateau regime. As seen, a densification regime follows the plateau regime's end. All of the following figure have their stress normalized by the by the density of foams (ρ_{rel}), to eliminate the density influence on the mechanical properties of the foams. Density-graded foams displayed a steeper plateau regime than the others, and merged foams exhibited the highest peak stress. The plateau regime for merged foams was shown to have a negative slope at greater relative densities (35%). The final graph of stress-strain curve (fig 34) is all of the previous curves of the samples combined, to make it easier for comparison and interpretation.

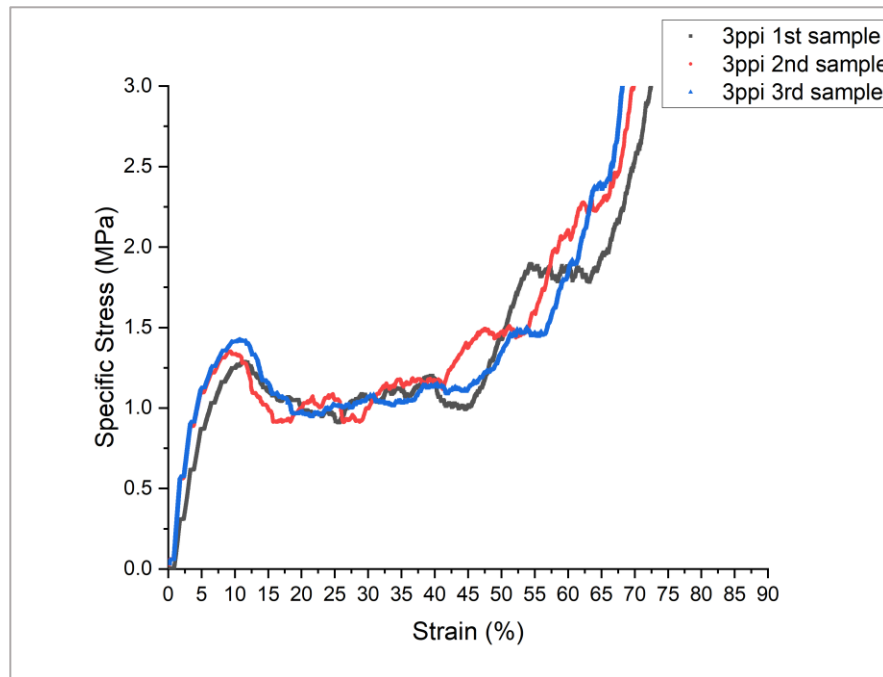


Figure 30 Specific stress, strain graph for 3ppi

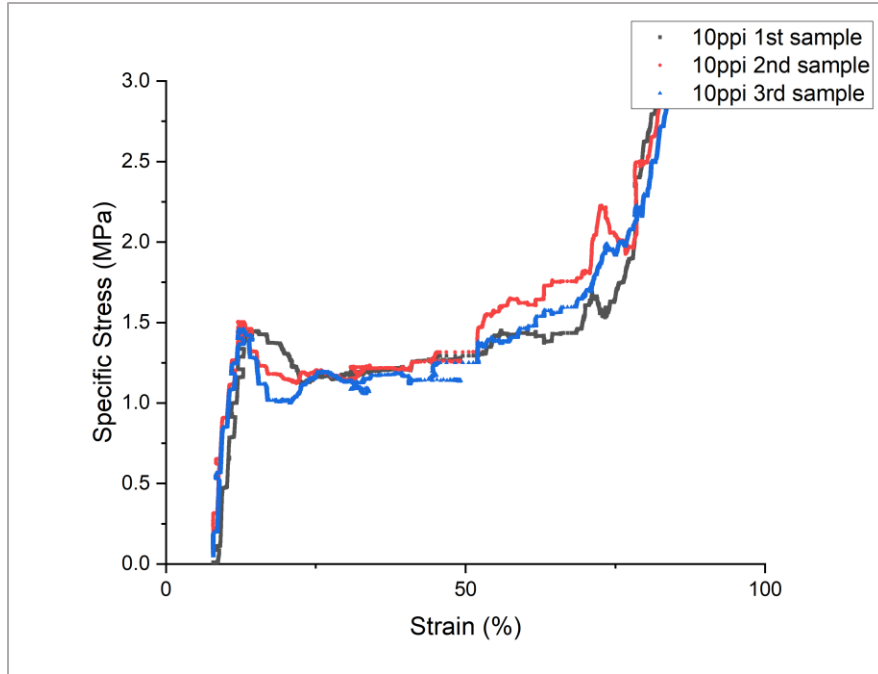


Figure 31 Specific stress, strain graph for 10ppi

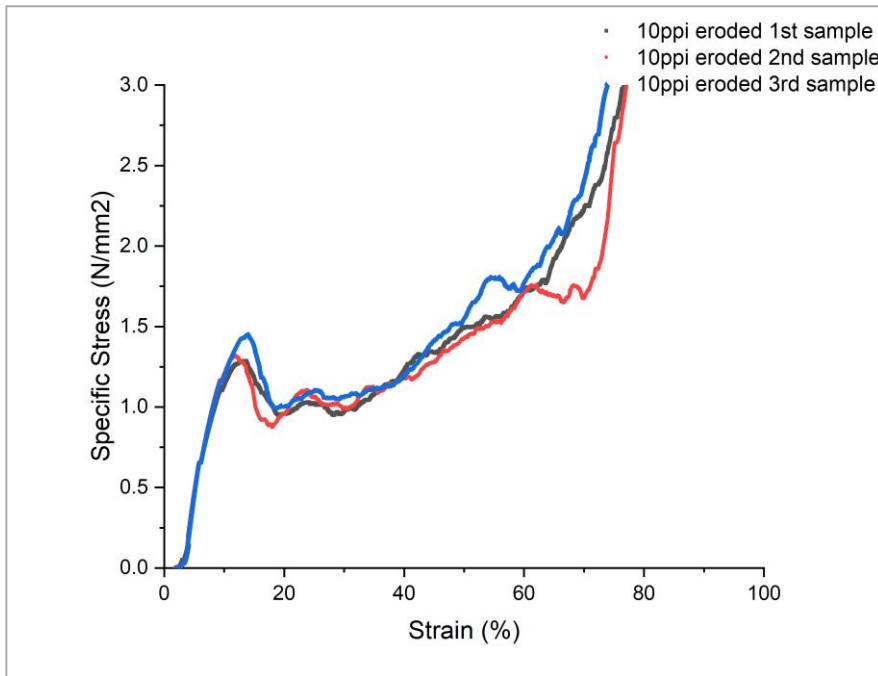


Figure 32 Specific stress, strain graph for eroded

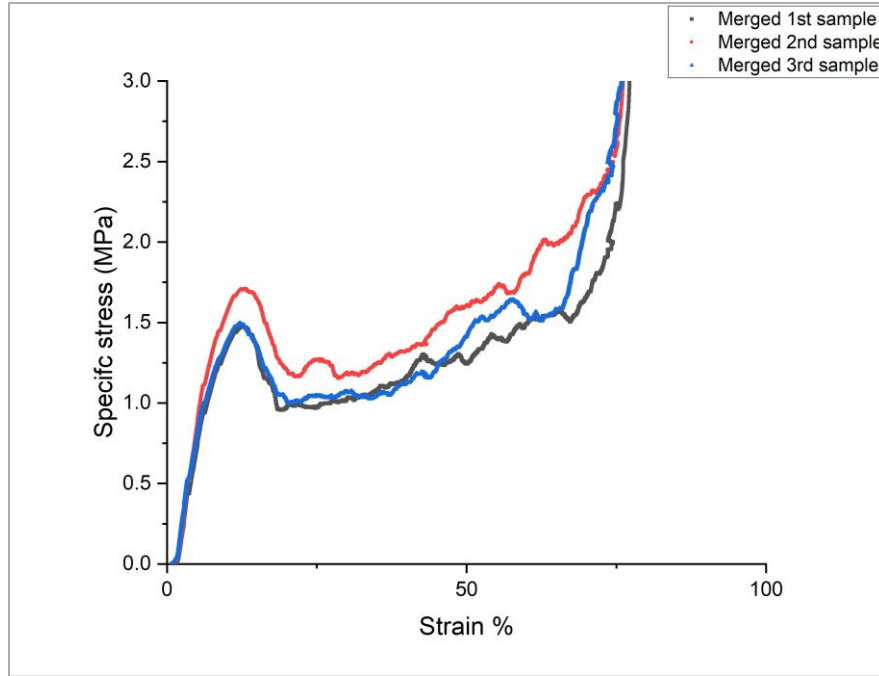


Figure 33 Specific stress, strain graph for merged-1

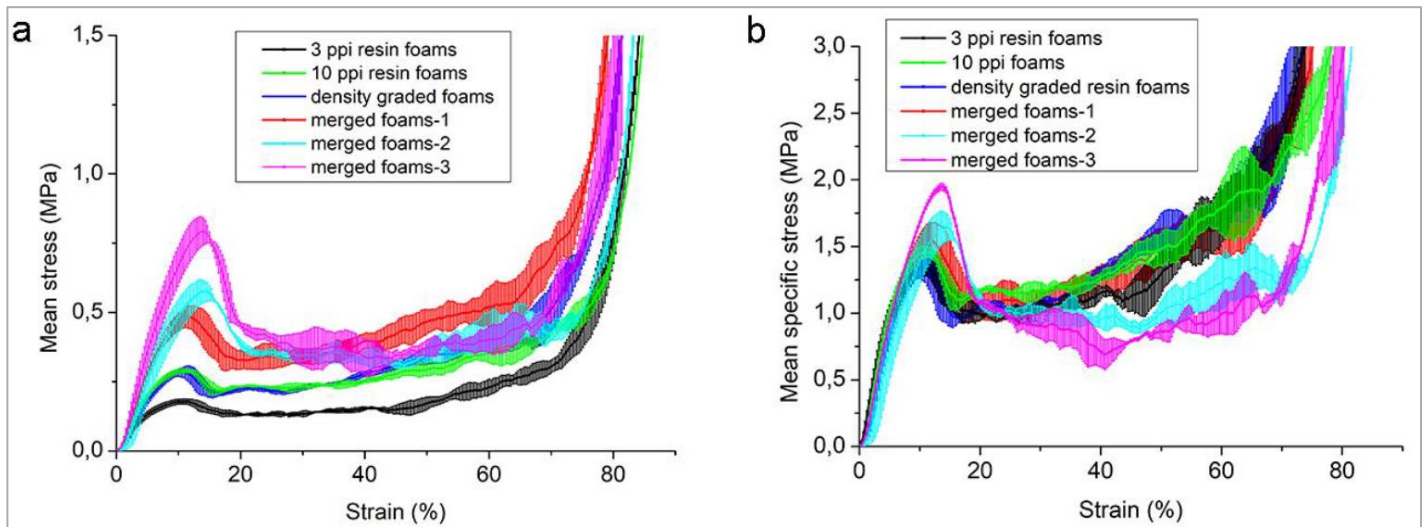


Figure 34 a) Mean stress-strain and b) specific stress-strain curves of printed 3, 10ppi, density graded, and merged resin foams.

4. FRACTURE OBSERVATIONS

Fracture observations in foams can vary depending on the type of foam, its composition, and the conditions under which it is subjected to stress. Here are some general observations related to foam fractures:

- **Brittle Fracture:** Some foams, particularly those with a high proportion of rigid or brittle materials, can exhibit brittle fracture behavior. In this case, the foam fails suddenly and without significant deformation, resulting in a clean break. Brittle fractures typically occur when the applied stress exceeds the foam's strength, leading to rapid crack propagation.
- **Ductile Fracture:** Certain foams, such as those with a higher proportion of flexible or elastomeric components, tend to exhibit ductile fracture behavior. Ductile fractures involve plastic deformation before the final separation of the foam. When subjected to stress, the foam deforms and elongates, showing signs of necking or thinning before ultimate failure.
- **Crack Propagation:** Foams may display crack propagation characteristics depending on their cellular structure. Cracks can propagate through cell walls, along cell boundaries, or a combination of both. The specific crack path depends on factors like foam density, cell size, cell wall thickness, and the presence of any reinforcing agents.
- **Shear Fracture:** In some cases, foams may undergo shear fracture, where the material breaks along a plane parallel to the direction of applied shear stress. This type of fracture is common when foams are subjected to shear forces, such as during impact or compression.
- **Delamination:** Delamination refers to the separation or splitting of printing layers, often occurring along the interface between different foam sections or between the foam and an adhered material. Delamination can result from inadequate bonding, stress concentration, or cyclic loading, among other factors.
- **Energy Absorption:** One of the advantageous properties of foams is their ability to absorb energy during fracture. When a foam fractures, the energy required to break the material is dissipated through various mechanisms, such as cell wall deformation, crack propagation, and crushing of foam structure. This energy absorption characteristic is particularly beneficial in applications where impact resistance or cushioning is essential.

It's important to note that these observations are general and can vary depending on the specific foam composition, manufacturing method, and testing conditions.

The strut surface of the tested materials was optically micrographed using a Zeiss Smartzoom 5 light microscope (Zeiss, Jena, Germany). During compression testing, a 2-megapixel CCD camera was used to examine the sample surface. Using a scanning electron microscope (SEM, Thermo Fisher Quattro ESEM FE-SEM, Waltham, USA), the fracture surfaces of the eight samples were examined. A secondary electron mode with a 2 kV accelerating voltage was used for imaging in the SEM.

During cell collapse in foam compression, struts bent and tore. Fracture surfaces are represented in SEM micrographs by the green rectangle, while deposition layer lines are denoted by an arrow. Deposition layer lines are positioned differently in each strut in relation to their cross-sections. For example, the cross-section of the strut indicated by the green rectangle is parallel to the lines of the deposited layer. The cross-section of the strut pointed at by the red arrow, on the other hand, is parallel to the lines of the deposited layer. The layer interface denoted by the asterisk "*" served as the fracture starting point. Smooth surface with brittle fracture surface was observed. The layer interface in the strut was represented by a valley; the crack started in the valley and spread in the radial direction of the strut.

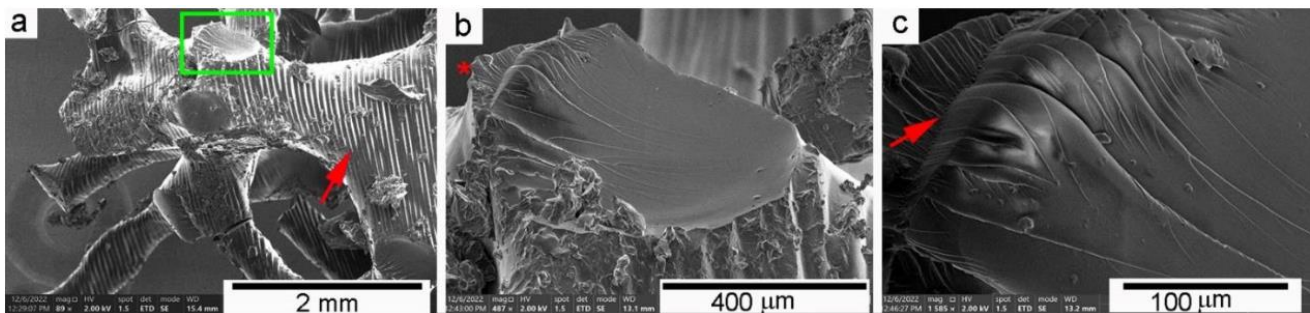


Figure 35 SEM micrograph of damaged strut

The first image has a fractured strut's surface which marked by a green rectangle, and layer lines are denoted by a red arrow (a). And in the second one (b), red asterisks "*" indicate the crack initiation point on the fracture surface of a strut. The last image with the valley formed at the layer interface is indicated by the red arrow in the magnified image of a fracture creation point (c).

5. RESULTS

Mechanical properties of resin foams, including peak stress, plateau stress, loading modulus, and densification strain, are determined as follows [23]:

- the loading modulus is measured as the slope within the linear deformation range between stresses of 10% and 60% of the peak stress.
- the peak stress is the maximum stress reached in the elastic regime, and before the plateau region starts.
- the plateau stress (crushing strength) is calculated as the average stress at a strain interval between 20% and 30%.
- the densification strain is determined as the strain at which the stress reaches 1.3 times the plateau stress.
- Energy absorption is determined by the applied force divided by the volume, accordingly mass. The energy absorbed per unit volume by the foam is the area under the stress- strain curve up to the densification strain.

The mechanical properties of the resin foams are outlined in table 9. Loading modulus, peak stress, plateau stress, and energy absorption per volume were heavily governed by the relative foam density, and merged foam exhibited the highest values for those properties. The 3ppi foams have the lowest energy absorption per mass while the merged-2 foams have the highest absorption per mass.

Table 9 Mechanical properties of the polymeric resin foams

<i>Samples</i>	<i>Loading modulus (MPa)</i>	<i>Peak stress (MPa)</i>	<i>Plateau stress (MPa)</i>	<i>Densification strain (%)</i>	<i>Energy absorption per volume (MJ/m³)</i>	<i>Energy absorption per mass (kJ/kg)</i>
<i>3ppi</i>	3.5±0.7	0.18±0.01	0.13±0.00	49.27±3.68	0.071±0.002	0.44±0.01
<i>10ppi</i>	5.5±0.2	0.29±0.01	0.22±0.01	50.44±4.73	0.117±0.003	0.49±0.01
<i>Merged-1</i>	8.1±0.6	0.49±0.04	0.34±0.04	46.68±1.13	0.179±0.016	0.47±0.04
<i>10ppi eroded</i>	4.7±0.2	0.29±0.02	0.22±0.01	40.55±2.56	0.120±0.004	0.46±0.01
<i>Merged-2</i>	6.9±0.5	0.57±0.03	0.33±0.04	65.46±8.37	0.290±0.030	0.68±0.07
<i>Merged-3</i>	8.9±1.6	0.80±0.05	0.41±0.02	69.96±1.12	0.343±0.067	0.67±0.13

The 10ppi eroded foams' densification strain revealed an unexpected outcome. The lowest densification strain was identified for the density-graded foams with lower relative density than merged foams.

The first collapse behavior in the stress-strain curves is determined by the ductility ratio (D). It is calculated as the ratio of the minimum stress; minimum stress is the sudden decrease of stress after peak stress to the peak stress. Once the D approaches 1, the cell collapse takes place more gradually.[19][20]

Merged foams with considerable peak stress showed the lowest ductility ratio. In contrast, 3 and 10ppi foams revealed the highest ductility ratio. 10ppi and merged foams exhibited the most increased normalized peak stress. In contrast, eroded and 3ppi foams showed the lowest.

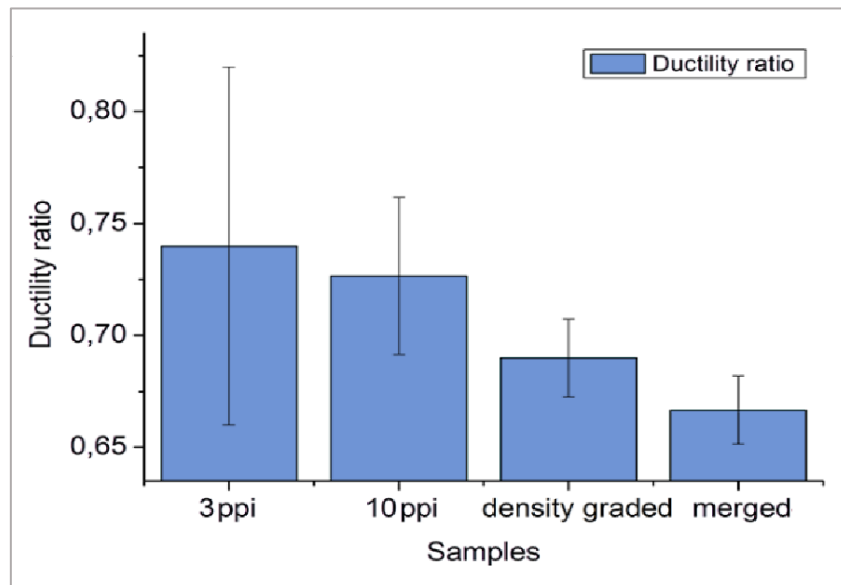


Figure 36 samples ductility ratio

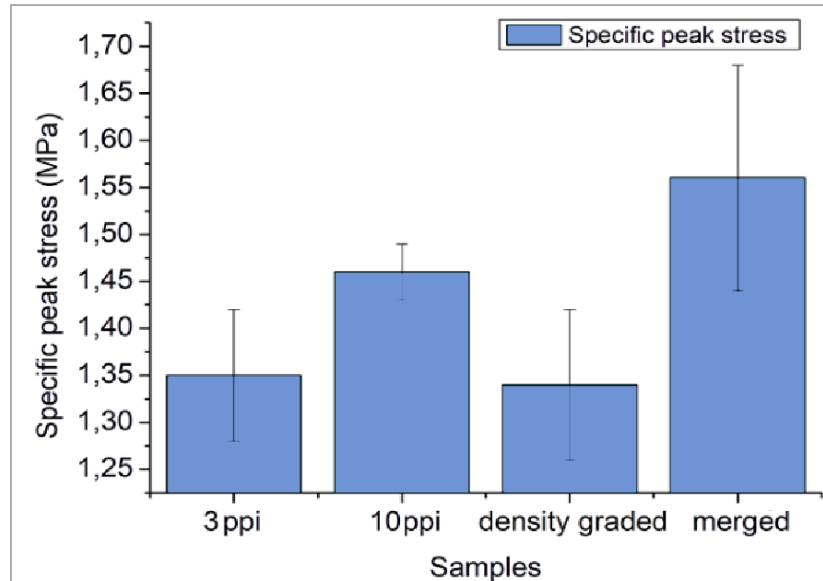


Figure 37 samples normalized peak stress

In conclusion, this master thesis on reverse-engineered foams has presented a comprehensive investigation into the principles and methodologies of this innovative approach in foam design and manufacturing. Through a combination of theoretical analysis, experimental studies, and computational modeling, this research has contributed to the understanding and advancement of reverse engineering techniques for foam materials.

The findings of this thesis have highlighted the significance of reverse engineering in the development of foams with tailored properties and performance characteristics. By deconstructing existing foam structures and analyzing their composition, morphology, and properties, it has been possible to extract valuable insights and parameters for the creation of new foam materials with desired attributes.

However, despite the advancements made in reverse-engineered foams, there are still avenues for further research and development. Exploring advanced characterization techniques, investigating more novel foam compositions, and optimizing manufacturing processes are essential areas for future investigation. Additionally, considerations for sustainability and environmental impact should be integrated into the development of reverse-engineered foams to ensure a more sustainable future.

In summary, this master thesis has contributed to the field of reverse-engineered foams by providing valuable insights into the principles, methodologies, and applications of this innovative approach. The research outcomes pave the way for advancements in foam materials, offering new possibilities for tailored foam design and manufacturing. The findings from this work hold promise for the development of next-generation foams that can address complex engineering challenges, revolutionize various industries, and drive innovation in the years to come.

6. DISCUSSION

Novel structure design

The following images are cells of 3D computed tomography rendered 3ppi, 10ppi and merged respectively. With reverse engineering it was possible to create novel structures by modifying existing models of other foams. Struts are connected by merging. They cross each other in various places. The complexity and irregularity of the foam cells increased as a result of merging, which changed the regular cell topology. The length of the struts is shortened where they intersect. Additionally, the merging of the foams reduces the connection angle of the nearby struts. There is no regular foam cell as seen in lattice systems because of the struts' interlocking. This makes it difficult to characterize the cell structure; an example might be to a 3D mesh of polygons.

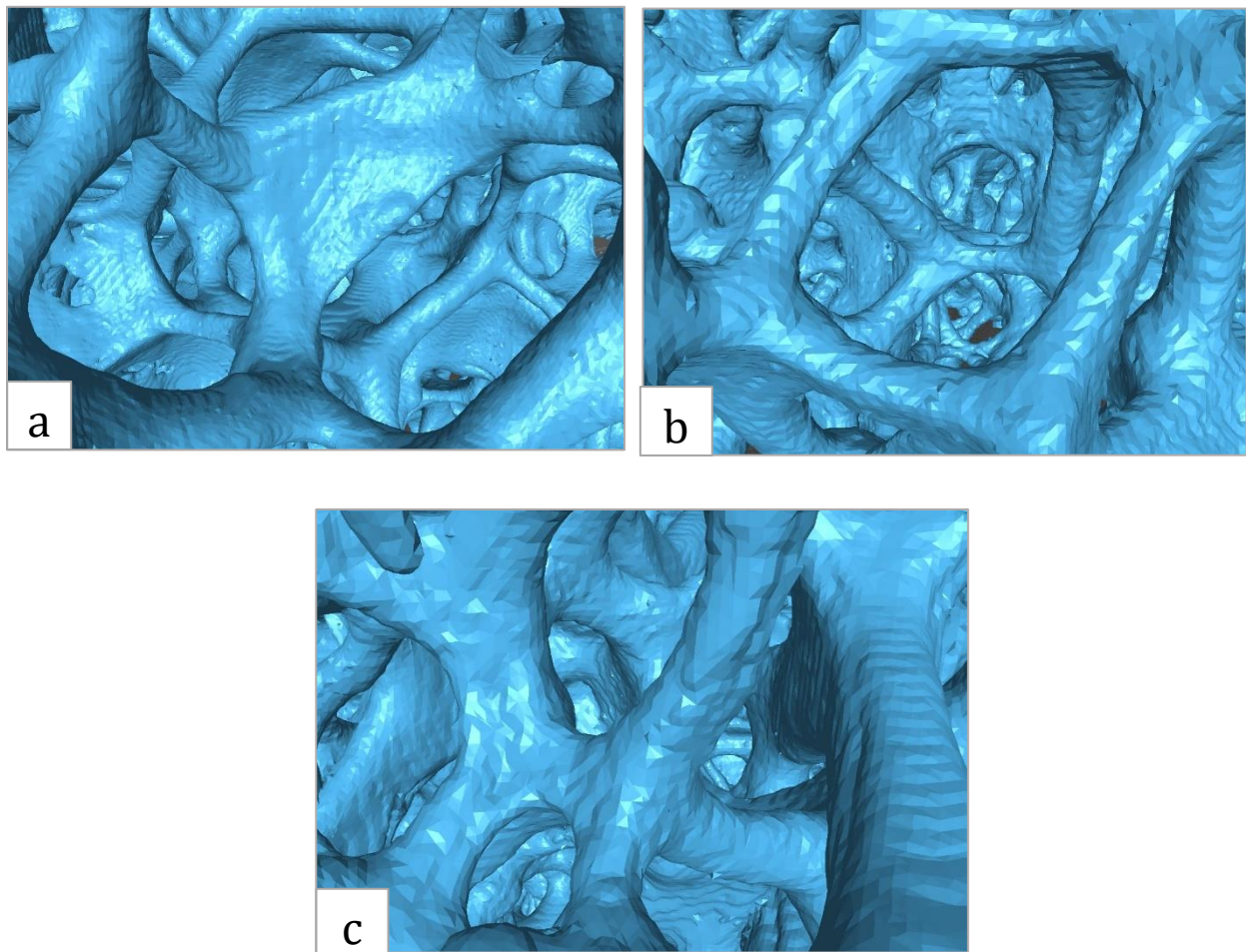


Figure 39 foam cells of a) 3ppi b) 10ppi and c) merged

Mechanical Properties of resin foams:

The primary determinant of the mechanical properties of foams is density. However, the stress-strain curve form of the foams is significantly influenced by the strut ductility and hardness. Brittle materials exhibit an extended plateau regime that greatly oscillates, and in other instances, no actual plateau regime is seen at all. Additionally, the connection between relative density and foam strength was modified for brittle resin foams. Therefore, the question of whether the mechanical property and relative density of brittle resin foams are correlated arises. The crushing strength of brittle foams is connected with their relative densities as follows, according to the Gibson-Ashby rule [43]:

$$\frac{\sigma_{cr}^*}{\sigma_{fs}} \approx C_1 \left(\frac{\rho^*}{\rho_s} \right)^{\frac{3}{2}} \quad (\text{eq.1})$$

where, σ_{cr}^* is the crushing strength of foam, σ_{fs} is the fracture strength of the struts and ρ^* is the foam density, ρ_s is the material density from which strut is made of. C_1 represents the constant of proportionality. C_1 was determined to be 0.2 for elastic-brittle foams. The exponent with $n = 1.5$ here indicates the bending dominating foam structure. Because the bending of the struts in the foam compression has been shown, this is true for resin foams in the present study.

The relationship between the elastic modulus and relative density of foams is linear. where E^* is the elastic modulus of the foams, and E_s is the elastic modulus of struts

$$\frac{E^*}{E_s} = \left(\frac{\rho^*}{\rho_s} \right)^2 \quad (\text{eq.2})$$

The following curve fitting was done using a power function after experimental results were plotted:

$$\frac{\sigma_{cr}^*}{\sigma_{fs}} \approx 0.08 \left(\frac{\rho^*}{\rho_s} \right)^{0.72} \quad (\text{eq.3})$$

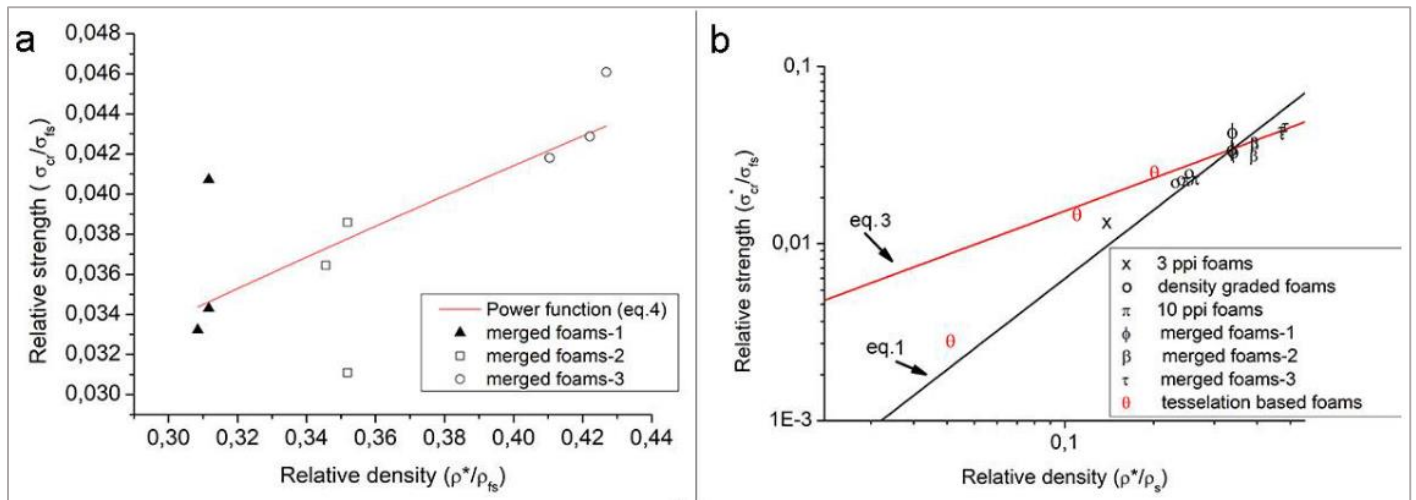


Figure 40 a) curve fitting of merging foams' experimental results b) Comparison of the Gibson-Ahby rule (eq.1) for all tested foams and the derived equation (eq.3) for merged foams

Plots demonstrating the relationship between the resin foams' relative strength and relative density: a) curve fitting of merging foams' experimental results and b) Comparison of the Gibson-Ahby rule (eq.1) for all tested foams and the derived equation (eq.3) for merged foams.

Intriguingly, the exponent ($n = 0.72$) in the current power function, which delivers the strut's deformation mode, indicated behavior that was stretch-dominated. The struts' interlocking caused by the merging of foams changed their deformation behavior, resulting in a behavior where stretch predominates. As the study's tessellation-based foam structure's foam density was raised, a bending-dominated foam structure emerged. The 3 and 10ppi foams' power exponents, which ranged from 0.9 to 1.2, showed bending-dominated behavior. Scale effects most likely had an impact on the strength in the case of 3ppi foam, causing a few deviations in the exponent.

Foam strength and the connection between relative densities were significantly affected through modifications to the foam's structure and density. In conclusion, the stretch-dominant foam structure for merged foams replaced the bending-dominant structure at 3 and 10ppi. Mechanical properties are adversely affected by density grading. For example, Chen et al. showed that graded foams had lower strength than uniform foams.

The density-graded foams in the current study have a lower normalized peak stress than the uniform 10ppi foams. According to the reference [7], this is accurate. In addition, Chen et al. reported that the strength of the foams reduced as topological disorder 15 was increased. The current study shows that merged foams have lower densification strain than 10ppi foams and higher normalized peak stress than 3ppi and eroded foams. This is explained by the merged foams' stretch-dominated nature. Stretch-dominated foams' stress-strain curves show softening after the peak stress, and this is connected to the foams' ductility ratio. The more softening after peak stress occurs, the lower the ductility ratio. The struts becoming entangled in the merged foams results in a higher peak stress. The strut length in the combined foams was decreased by the digital intersection of the struts in CT slices. Shorter struts experience less bending moment, which results in stronger foams that can support greater forces. Uniform 10ppi foams were more durable than 3ppi foams because of the size effect. When there are less than six cells in one dimension, strength is reduced. 5–6 cells can be detected in one dimension of 3ppi foams. [44][10]

The fact that the densification strain for density-graded foams is lower than for 10ppi foams is another important outcome. The compaction and densification of the struts occurred at lower strains because the strut thickness was raised five times in the region of interest, which was designated by a rectangle in the center of the foams. As a result, the plateau regime of stress-strain curves exhibits a sharp increase. In the plateau regime, stress appears to have decreased due to the reduction of voids in the cellular structure, which caused severe fracturing and cell collapse. In contrast, the squeeze of the struts in the cell voids causes the stress to rise at low densities for 10, 3, and graded foams.

Damage mechanisms of resin foams:

Deformation band formation is influenced by the foam's cell size, density, and structure. For 10ppi and density-graded foams, cell size and design are comparable, and as a result, cell collapse behavior is also similar. When it comes to 3ppi foams, cell collapse only affects a small area around it, deformation bands don't run the full width of the foam, and stress remains nearly constant during the plateau period (strain up to 40%). This is explained by the fact that struts can be compacted in the big voids in the cell structures. For merged foams, as opposed to 10ppi and density-graded foams, deformation bands spread perpendicular to the loading axis. At the macroscale, cell structure modification affects how foams deform.

The fabrication method has a major impact on the strut damage processes at the microscale. A layer interface between two adjacent layers develops as a result of the struts being printed layerwise. Due to the thin connection between the layers, the crack generally starts at this interface. While the orientation of the layer interface is noticeable and constant for bulk materials, it is different for each foam strut. This may result in a single strut undergoing constrained deformation. Cracking may start if the layer orientation favors the direction of the applied forces, leading to an early cell collapse. Anisotropic cell collapse behavior may result from this.

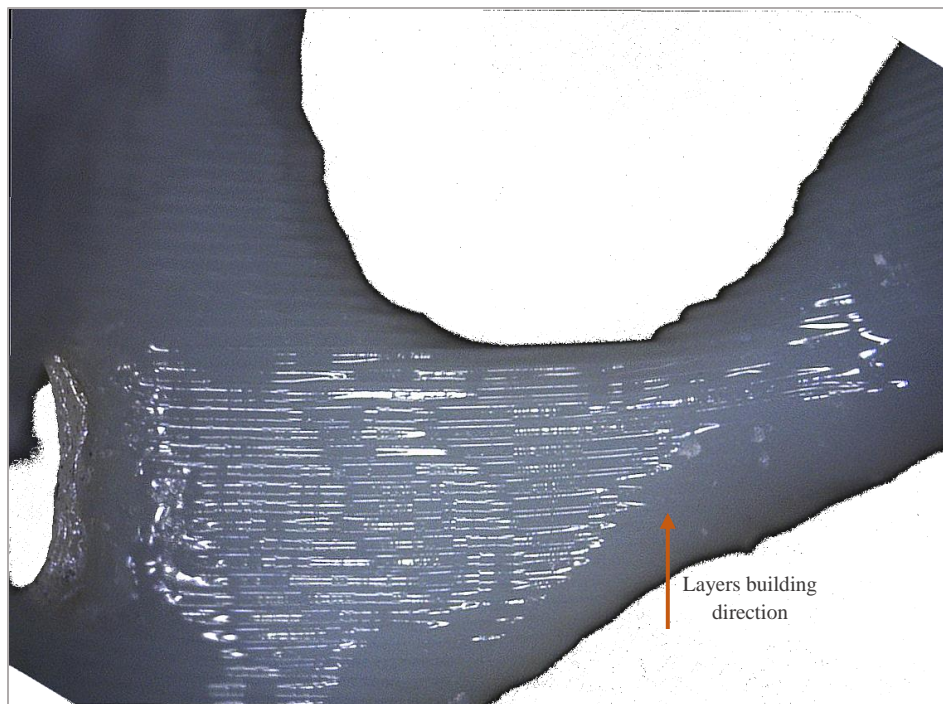


Figure 42 Layers printing direction

At the macroscale, cell structure modification affects how foams deform. SLA was used by Ling et al. to create polymeric resin octet-truss lattice specimens. They also demonstrated that the plateau curve was flattened as strut thickness was increased. According to them, the buckling happened more abruptly for thinner struts and more consistently for thicker struts. In contrast, when the density of the merged foams increased, the plateau regime fluctuated and the struts suffered a severe fracture as a result of the localized deformation. Additionally, Ling et al.'s research demonstrated that durable resin foams are ductile due to their extended plateau regime, in contrast to typical grey resin foams which are brittle due to their lack of an extended plateau regime. The brittle fracture of the resin struts and fluctuations in the plateau regime that result in a brittle foam were seen in the present study, as was the case for carbon foams in. [25-26]

Open-cell resin foams behave differently when deformed than the original steel foams. Because of their austenitic microstructure, steel foams underwent significant strain hardening in the plateau regime, whereas resin foams did not. Resin foams also have a high peak stress that is followed by easing of the strain. Steel foams, in contrast, exhibited no peak stress. The base material affects the mechanical characteristics and deformation behavior of the foams despite having the same cell structure. [42]

The following drawing showing the layer orientation in relation to the strut section in a strut node of an open cell foam. The printing layer can be positioned vertically, parallel to the strut sections, or tilted.

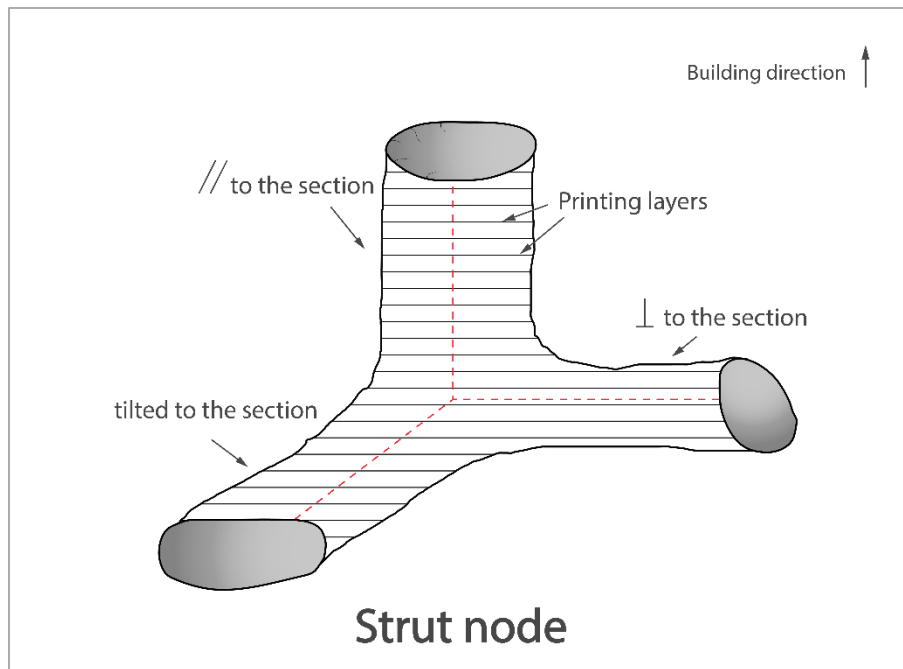


Figure 43 layer positioning in relation to a strut node's strut section in an open cell foam

7. CONCLUSION

In this study, complex novel foam structures were made through reverse engineering. To create resin foams, CT images of steel foams with 30 and 45ppi were processed, resized, and turned into an.obj file. An MSLA printer was used to create foams that were 3, 10ppi, density graded, and merged (from 3 and 10ppi). Compression testing was used to observe and assess their mechanical performance, and optical and electron microscopes were used to examine damage.

The following conclusions can be made based from those observations:

- Without the need of support materials, reverse engineering has been effectively implemented and conducted. Micro details like the hollow in the struts and the cross-sections of the struts, however, could not be completely replicated in the resin foams.
- The mechanical properties are negatively impacted by density grading: the peak stress of normalized foam is lower than that of uniform 10ppi foams, and densification strain decreased because of the high slope in the plateau regime.
- Digitally merging two foams caused the bending-dominated structures to change into stretch-dominated structures. Peak stress increased, although softening resulted in a decrease in energy absorption per mass.
- Compared to metal foams made using conventional methods of manufacturing, reverse-engineered foams have less scattering in their mechanical characteristics.
- An increase in the relative density of merged foams leads to higher energy absorption per mass and densification strain.
- The damage to the foam strut was significantly impacted by the foams' building direction. The layer interface's orientation to the strut elongation axis varies in each strut.

In light of the research conducted in this study on reverse-engineered foams, several promising avenues for future exploration and development can be identified. These outlooks serve as a roadmap for further advancements and applications in the field, offering opportunities to enhance the understanding, capabilities, and practical implementation of reverse-engineering techniques for foam materials.

- **Advanced Characterization Techniques:** Future research should focus on the development and utilization of advanced characterization techniques to gain deeper insights into the microstructure and properties of reverse-engineered foams. Techniques such as high-resolution microscopy, X-ray imaging, and spectroscopy can provide valuable information about cell morphology, distribution, and chemical composition, enabling more precise control over foam design and performance.
- **Tailoring Foam Properties:** The future of reverse-engineered foams lies in the ability to precisely tailor their properties to meet specific application requirements. Further investigation is needed to explore the influence of different variables, such as cell size, shape, and connectivity, on foam performance. This includes understanding the effects of material selection and processing conditions on the resulting foam properties.
- **Process Optimization and Scale-up:** Efficient and cost-effective manufacturing processes are crucial for the practical implementation of reverse-engineered foams. Future research should focus on process optimization, scalability, and automation to ensure the reproducibility and commercial viability of these advanced foam materials.

By pursuing these future outlooks, researchers and engineers can continue to push the boundaries of reverse-engineered foams, unlocking new possibilities for tailored foam design, performance optimization, and widespread industrial applications. Through interdisciplinary collaboration and a commitment to sustainable practices, the field of reverse-engineered foams will continue to evolve, making significant contributions to various sectors and addressing complex engineering challenges in the years ahead.

8. REFERENCES

1. Banhart, J., Manufacture, characterization and application of cellular metals and metal foams. *Progress in Materials Science*, (2001), 559-632.
2. Ashby, M. F., Evans, A. G., Fleck, N. A., Gibson, L. J., & Hutchinson, J. W. *Metal Foams: A Design Guide*. Butterworth-Heinemann (2000).
3. Kumar, M., & Gupta, N. A review on metallic foams: fabrication, properties, and applications. *Journal of Materials Science*, (2017), 52(12), 6917-6947. doi:10.1007/s10853-017-0852-1
4. Gibson, L. J., & Ashby, M. F., *Cellular solids: Structure and properties*. Cambridge University Press. (1999)
5. Baumeister, J., Baumeister, T., & Earl, W., *Metallic foam: design, properties and applications*. *Advanced Engineering Materials*, (2006), 8(9), 781-794. doi:10.1002/adem.200600103
6. Li, Y., & Chen, X. *Metallic Foams: Current Status and Future Perspectives*. *Advanced Materials Interfaces*, (2016), 3(7), 1500811. doi:10.1002/admi.201500811
7. E Chen, S Luan, S Gaitanaros, On the strength of brittle foams with uniform and gradient densities, *Extreme Mech. Lett.*,51 (2022) 101598.
8. S Bi, E Chen, S. Gaitanaros, Additive manufacturing and characterization of brittle foams, *Mech. Mater.* 145 (2020) 103368
9. Fleck, N. A., *Metal foams: a tutorial*. *Applied Mechanics Reviews*, (2009), 62(2), 020802. doi:10.1115/1.3072889
10. E. Chen, S. Luan, S. Gaitanaros, On the compressive strength of brittle lattice metamaterials, *Int. J. Solids Struct.*, 257 (2022) 111871.
11. H. Jiang, H. Ziegler, Z. Zhang, S. Atre, Y. Chen, Bending behavior of 3D printed mechanically robust tubular lattice metamaterials, *Addit. Manuf.*, 50 (2022) 102565.
12. L.E. Murr, S.M. Gaytan, F. Medina, E. Martinez, J.L. Martinez, D.H. Hernandez, B.I. Machado, D.A. Ramirez, R.B. Wicker, Characterization of Ti–6Al–4V open cellular foams fabricated by additive manufacturing using electron beam melting, *Mater. Sci. Eng. A* 527 (2010) 1861-1868.
13. Y-J Hwang, K-S Kim, B AlMangour, D Grzesiak, K-A Lee, A New Approach for Manufacturing Stochastic Pure Magnesium Foam by Laser Powder Bed Fusion:

- Fabrication, Geometrical Characteristics, and Compressive Mechanical Properties, *Adv. Eng. Mater.*, 23 (2021) 2100483.
14. E. Hernández-Nava, C.J. Smith, F. Derguti, S. Tammam-Williams, F. Léonard, P.J. Withers, I. Todd, R. Goodall, The effect of density and feature size on mechanical properties of isostructural metallic foams produced by additive manufacturing, *Acta Mater.*, 85 (2015) 387-395.
 15. JRC Dizon, AH Espera Jr, Q Chen, RC Advincula, Mechanical characterization of 3D-printed polymers, *Addit. Manuf.*, 20 (2018) 44-67.
 16. Rüggeberg, M., Trabandt, S., & Weise, J. (2014). X-ray computed tomography of polymer foams: A review. *Polymer Testing*, 38, 139-154. doi:10.1016/j.polymertesting.2014.05.005
 17. Bodey, A. J., Sinclair, I., & Spearing, S. M. (2012). The use of X-ray computed tomography in the characterisation of cellular materials. *Materials Science and Engineering: R: Reports*, 74(12), 377-399. doi:10.1016/j.mser.2013.02.001
 18. Precision Universal Testing Machines AUTOGRAPH AGX-V Series, Shimadzu
 19. M Firoozbakht, A Blond, G Zimmermann, A C Kaya, C Fleck, A Bührig-Polaczek, Analyzing the influence of the investment casting process parameters on microstructure and mechanical properties of open-pore Al–7Si foams, *J. Mater Res. Technol*, 23 (2023) 2123-2135
 20. N. Dukhan (Ed.), *Proceedings of the 11th international conference on porous metals and metallic foams (MetFoam 2019)*, Springer (2019)
 21. N. Movahedi, I. V. Belova, G. E. Murch & T. Fiedler, Functionally Graded Syntactic Foams with Layers of Dissimilar Metallic Matrices, *J. Mater. Eng. Perform*, 31 (2022) 1058–1065.
 22. K A Mustapha, F S Anuar, and F A-Z M Saat, Prediction of Slip Velocity at the Interface of Open-Cell Metal Foam Using 3D Printed Foams, *Colloid Interfaces*, 6 (2022) 80
 23. ISO 13314:2011 Mechanical testing of metals - Ductility testing - Compression test for porous and cellular metals, 77 (40) (2011), p. 10
 24. K. Salonitis, Stereolithography. *Comprehensive Materials Processing*, 19–67. doi:10.1016/b978-0-08-096532-1.01001-3 In book: *Comprehensive Materials Processing Chapter*, Elsevier, Editors: Saleem Hashmi (2014).
 25. A. Celzard, W. Zhao, A. Pizzi, V. Fierro, Mechanical properties of tannin-based rigid foams undergoing compression, *Mater Sci Eng A*, 527 (2010) 4438-4446

26. C. Ling, A. Cernicchi, M.D. Gilchrist, P. Cardiff, Mechanical behaviour of additively-manufactured polymeric octet-truss lattice structures under quasi-static and dynamic compressive loading, *Mater Design* 162 (2019) 106–118.
27. C Tang, J Liu, Y Yang, Y Liu, S Jiang, W Hao, Effect of process parameters on mechanical properties of 3D printed PLA lattice structures, *Composites Part C*, 3 (2020).
28. Yi Zhang*, William Jarosinski**, Yeon-Gil Jung†, Jing Zhang*, Additive manufacturing processes and equipment, (2018), (40- 44)
29. Wong KV, Hernandez A. A review of additive manufacturing. *ISRN Mech. Eng.* 2012.
30. Várady, T., Martin, R. R., & Cox, J. (1997). Reverse engineering of geometric models, an introduction. *Computer-Aided Design*, 29(4), 255–268.
31. Špelic, I. (2019). The current status on 3D scanning and CAD/CAM applications in textile research. *International Journal of Clothing Science and Technology*, 32(6), 891–907
32. Lan P-T, et al. Determining fabrication orientations for rapid prototyping with Stereolithography apparatus. *Computer. Aided Des.* 1997;29(1):53–62
33. Schaub DA, Chu K-R, Montgomery DC. Optimizing stereolithography throughput. *J. Manuf. Syst.* 1997;16(4):290–303.
34. P. DUDEK, FDM 3D printing technology in manufacturing composite elements, (2013), 1-4
35. Jain, P., & Kuthe, A. M., Feasibility Study of Manufacturing Using Rapid Prototyping: FDM Approach. *Procedia Engineering*, (2013) 63, 4–11
36. Charoo, N. A., Barakh Ali, S. F., Mohamed, E. M., Kuttolamadom, M. A., Ozkan, T., Khan, M. A., & Rahman, Z. (2020). Selective Laser Sintering 3D Printing – An Overview of the Technology and Pharmaceutical Applications. *Drug Development and Industrial Pharmacy*, 1–26.
37. Nikolay K. Tolochko, et al., "Mechanisms of selective laser sintering and heat transfer in Ti powder", *Rapid Prototyping Journal*, Vol. 9 Iss:, (2003), 5 pp. 314-326
38. J.P. Kruth, X. Wang, et al., "Lasers and materials in selective laser sintering", *Assembly Automation*, Vol. 23 Iss:, (2003), 4 pp. 357 – 371
39. Wilhite, R., & Wölfel, I., 3D Printing for veterinary anatomy: An overview. *Anatomia, Histologia, Embryologia*, (2019), 48(6), 609–620.
40. 3dprinterly, What Types of SLA Resin Are There For 3D Printing? Best Brands & Types, 20 Apr. 2023, <https://3dprinterly.com/what-types-of-resin-are-there-for-3d-printing-best->

brands-types/

41. Paul Stevenson, Foam Engineering: Fundamentals and Applications, (2012)
42. A.C. Kaya, C. Fleck, Deformation behavior of open-cell stainless steel foams, Mater Sci and Eng: A 615 (2014) 447-456
43. L. J. Gibson, M. Ashby, Cellular Solids: Structure and Properties, 2nd ed., Cambridge University Press, Cambridge, United Kingdom, 1997
44. E.W. Andrews, G. Gioux, P. Onck, L.J. Gibson, Size effects in ductile cellular solids. Part II: experimental results, Int J Mech Sci, 43 (2001) 701-713.